



OPEN

DATA DESCRIPTOR

A multi-year, seasonally resolved dataset of Seaglider observations at Station ALOHA in the North Pacific Subtropical Gyre

Catherine A. Garcia ^{1,2}✉, Benedetto Barone ^{1,2}, Sara Ferrón ^{1,2}, Steve Poulos^{1,2} & David M. Karl ^{1,2}

We present a large, quality-controlled dataset consisting of autonomous underwater measurements of hydrographical (temperature, salinity, and pressure), chemical (dissolved oxygen concentration), and bio-optical (chlorophyll *a* concentration and particulate backscatter) properties. Data were collected using underwater gliders on 18 missions in the North Pacific Subtropical Gyre between 2008 and 2023 (>20,000 vertical profiles). Each mission was centered near the long-term sampling site of the Hawaii Ocean Time-series program, Station ALOHA (A Long-term Oligotrophic Habitat Assessment). Measurements were quality controlled and calibrated to provide a robust dataset, inter-comparable among missions. We compare depth-resolved seasonality of Seaglider observations to previously described seasonal climatologies at Station ALOHA from ship-based observations. Results show that underwater gliders can accurately characterize ocean physical and biogeochemical conditions, reconstruct seasonality, and observe spatial variability and stochastic events in the absence of extensive ship operations. Further, these data allow us to study the variability of features, such as the chlorophyll and oxygen subsurface maxima with a temporal resolution of a few hours during multiple months.

Background & Summary

Seasonal oscillations, stochastic events, and spatial variability of biological phenomena are difficult to characterize in persistently stratified, oligotrophic habitats such as the center of subtropical gyres without extensive observational datasets. Subtropical gyres are characterized by year-round high light, warm temperatures, and low inorganic nutrient availability in the upper euphotic zone. However, conditions do vary on multiple temporal and spatial scales making low frequency observations – even monthly – difficult to interpret¹. While surface features (e.g. temperature and chlorophyll *a*) can be studied year-round with remote sensing, satellites fail to see the ocean below the surface layer.

The Hawaii Ocean Time-series (HOT) is a quasi-monthly, shipboard observation program established in 1988 to measure temporal variability of carbon production and fluxes, in the North Pacific Subtropical Gyre (NPSG) at Station ALOHA (22°45'N, 158°W)². Physical and biogeochemical processes are difficult to interpret without high frequency observations, and difficult to predict at a large scale without long-term observations³. For example, climatological comparisons of primary productivity to particle flux observations are correlated at Station ALOHA, while direct comparisons are not^{1,4}. Overcoming observational space-time lags is difficult as *in situ* observations at sea are labor and time intensive, and generally cost-prohibitive.

Autonomous underwater platforms (AUVs, e.g. underwater gliders and profiling floats) sample at high resolution over extended time-space scales (Fig. 1). Recently, temporal changes in both oxygen and bio-optical properties measured by autonomous floats and gliders have been used to estimate gross oxygen production and community primary production^{5–8}. Bio-optical properties have also been used to estimate particulate carbon fluxes^{9–12}. A complementary time-series of AUVs at Station ALOHA can potentially resolve lags between

¹Daniel K. Inouye Center for Microbial Oceanography: Research and Education (C-MORE), Honolulu, Hawaii, USA.

²Department of Oceanography, University of Hawai'i at Mānoa, Honolulu, Hawaii, USA. ✉e-mail: cathy.garcia@hawaii.edu

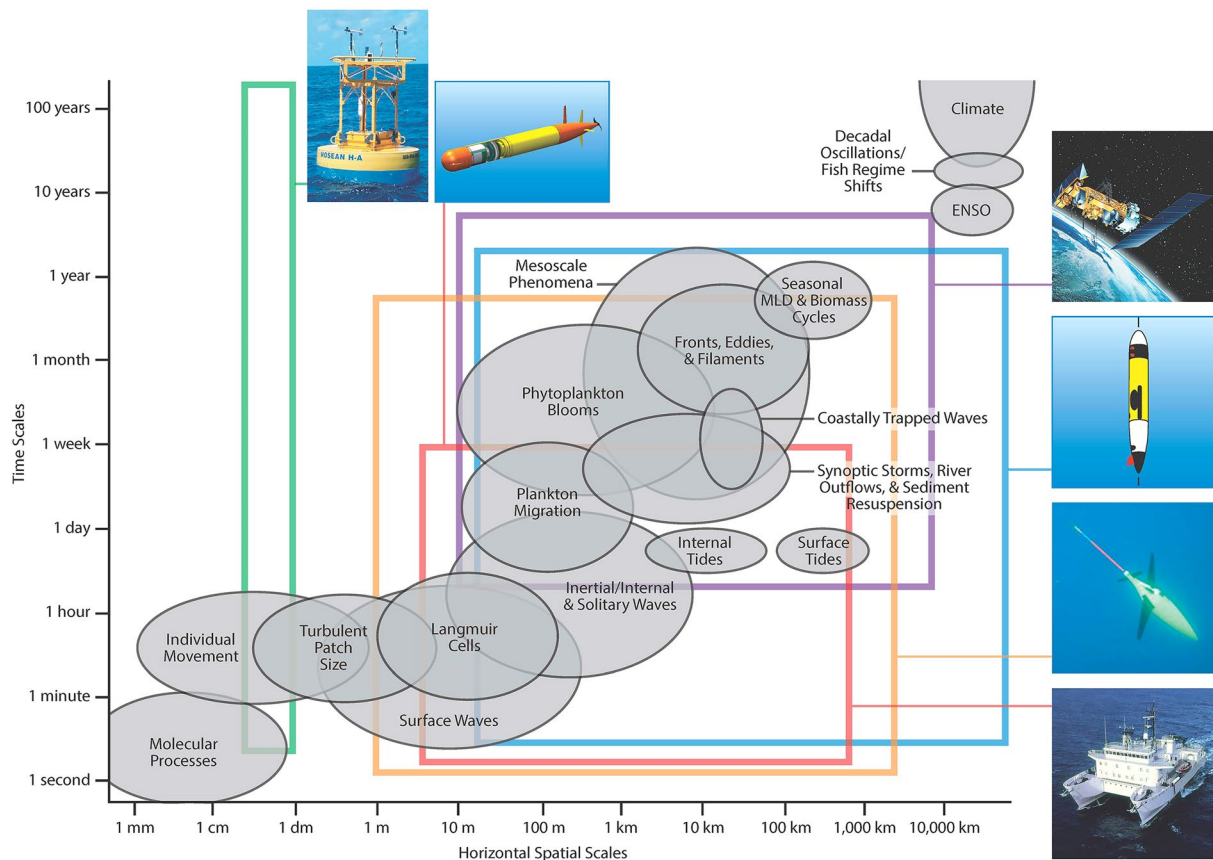


Fig. 1 Stommel-like diagram of cross-scale time and space continuum for observational platforms and ocean phenomena. Figure is reused with permission from Karl & Church³⁹, which was originally adapted from Stommel⁴⁶ and Dickey⁴⁷.

estimates of production and particle flux observations¹, as well as provide physical water column information influencing the bio-optical and chemical states over time. By leveraging the comparison of autonomous and shipboard observations, this study serves as a proof of concept for checking the feasibility of using underwater gliders for characterizing ocean conditions when shipboard measurements are either not available or too infrequent.

Since 2008, underwater gliders (Seaglider) have been regularly deployed in the vicinity of Station ALOHA (Fig. 2, Table 1). Seagliders are autonomous underwater vehicles that take high frequency (up to 0.2 Hz in our dataset), depth-resolved observations over several months and can be used to map large spatial features¹³. The gliders depicted in this study were equipped with sensors to measure temperature, salinity, pressure, dissolved oxygen concentration (O_2), chlorophyll *a* concentration (Chl *a*) from fluorescence (excitation/emission $\lambda = 470/695$ nm), and the particulate backscattering coefficient (b_{pp}) at three wavelengths ($\lambda = 470$ nm, 700 nm, and either 650 or 660 nm depending upon mission). Vertical profiles down to at least 200 m were collected for all sensors over periods of several months per mission (Table 1). This dataset comprises 18 missions between 2008 and 2023 centered on Station ALOHA, totaling over 20,000 depth profiles. Deployments and recoveries occurred during oceanographic cruises where water was collected at different depths and used to obtain precise and accurate laboratory measurements of the concentrations of O_2 , Chl *a*, and particulate carbon (PC) used for calibration and validation of the Seaglider dataset.

The raw observations were quality-controlled, accounting for known sensor responses and deviations from factory calibrations. As such, we provide a comprehensive Seaglider dataset that is inter-comparable among missions. Detailed descriptions of the data processing, quality control metrics, and calibration methods are provided herein. All quality control flags and adjustments (i.e. calibration and correction parameters) are preserved for the user. Only quality controlled data were used for technical validation.

A unique feature of this dataset is year-round coverage of a site overlapping a multi-decade time series operating since 1988. We evaluate the ability of Seagliders to reconstruct seasonal trends to 200 m compared to long-term, ship-based observations. There are few sites where gliders are used routinely at the same location in a subtropical gyre, apart from the Bermuda Atlantic Time-Series Study: <https://magic.bios.asu.edu/>. This allows for exploration of the influence of subseasonal processes (e.g. mesoscale and submesoscale motions, or atmospheric perturbations) that drive deviations from the seasonal means. The data presented here are available without restrictions at the Zenodo open access research data repository (<https://doi.org/10.5281/zenodo.14680626>)¹⁴. Version v1.2 of this dataset has been peer reviewed and used for all figures and tables within.

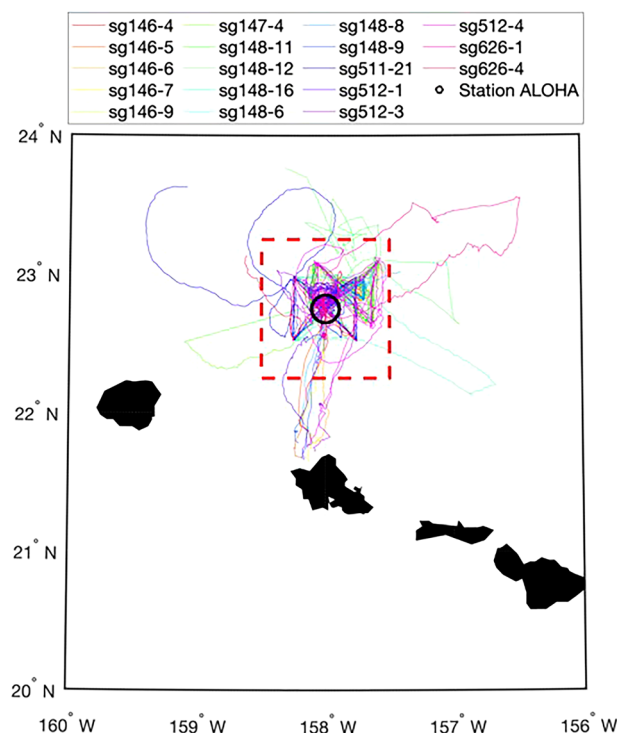


Fig. 2 Trajectories of the Seaglider missions near Station ALOHA. Black regions depict the Hawaiian Islands. Seasonal comparisons to observations at Station ALOHA (22°45'N, 158°W – black circle) are made using profiles within a 0.5 degree of latitude and longitude from the center of the sampling station (red outlined box).

Seaglider, Mission #	Date Start	Date End	#Profiles	Maximum Depth of Data Collection (m)			
				CT Sail	Aanderaa optode	Sea-Bird FLBB2	Sea-Bird FL2BB
sg146-4	13-May-2009	30-Jun-2009	434	908	906	202	202
sg146-5	14-Aug-2010	18-Nov-2010	1332	958	956	202	202
sg146-6	11-May-2011	4-Aug-2011	1254	908	907	501	202
sg146-7	23-May-2012	10-Jul-2012	632	707	707	202	202
sg146-9	13-Mar-2014	14-May-2014	684	807	806	602	602
sg148-6	14-Aug-2008	12-Oct-2008	984	519	519	202	202
sg147-4	25-Jul-2009	6-Nov-2009	1366	708	304	602	602
sg148-8	13-May-2009	23-Jul-2009	1076	909	907	201	201
sg148-9	10-Nov-2010	10-Feb-2011	1300	999	999	202	202
sg148-11	23-May-2012	9-Sep-2012	1204	759	757	204	204
sg148-12	24-May-2013	5-Sep-2013	956	913	909	909	909
sg148-16	3-Sep-2020	19-Nov-2020	1200	806	508	401	401
sg511-21	29-Mar-2023	13-Aug-2023	1860	713	713	617	617
sg512-1	15-Dec-2010	25-Mar-2011	2090	1039	1015*	206	1025
sg512-3	6-Aug-2012	23-Nov-2012	1538	907	907	203	907
sg512-4	19-Sep-2013	13-Dec-2013	866	912	912	909	912
sg626-1	26-Jan-2017	28-Apr-2017	1336	713	713*	202	202
sg626-4	26-May-2023	29-Jul-2023	892	811	808	810	810

Table 1. Seaglider mission dates, number of vertical profiles, and maximum collection depths. *Fast-response foil used in Aanderaa optode – all oxygen flagged as probably bad (see text).

Methods

Seagliders, guided AUVs developed at the University of Washington's Applied Physics lab¹³, were piloted either in a circular or 'bowtie' pattern for several months. Every set of dive profiles (i.e. the data collected between surfacing) was stored in individual files. Vertical profiles were processed individually and separated into those collected while the glider was descending and ascending. Upon completion of processing, all dive profiles were merged into a file for each mission. A complete list of variables available for most missions is listed in Table 2.

Variable Long name	Short Name in file	Units or Value	Description
Latitude	lat	decimal degrees	Decimal degrees north [−90,90]
Longitude	lon	decimal degrees	Decimal degrees east [−180,180]
Datetime	datetimeUTC	datetime UTC	Datetime format 'yyyy-mm-ddThh:mm:ss' Example: 2010-03-28T18:35:31' in UTC
Dive number	divenum	#	Dive number of combined descending and ascending profiles
Profile direction	vertical_direction	'up' or 'down'	Indicator of ascent 'up' or descent 'down'
Pitch angle	pitch	°	Angle of glider pitch relative to sea surface
Pressure	press	db	Pressure from Paine electronics or Kistler sensor
Depth	depth	m	Depth converted from Seaglider processing
Temperature	temp	°C	Sea-Bird CT Sail temperature corrected for 1 st order lag
Conductivity	cond	mS cm ^{−1}	Sea-Bird CT Sail conductivity corrected for 1 st order lag
Absolute salinity	salin	g kg ^{−1}	Absolute salinity calculated using Gibbs Seawater Toolbox v3.06.12
Potential density anomaly at 0 dbar	sigma	kg m ^{−3}	Potential density anomaly calculated using Gibbs Seawater Toolbox v3.06.12
Raw dissolved oxygen concentration	oxygen_raw	μmol L ^{−1}	Aanderaa oxygen output
Dissolved oxygen concentration	oxygen	μmol L ^{−1}	Aanderaa oxygen output, with inverse filter & calibration
Raw Chlorophyll <i>a</i> concentration	chl_a_raw	mg m ^{−3}	Sea-Bird ECO Puck chlorophyll <i>a</i> fluorescence converted to concentration
Chlorophyll <i>a</i> concentration	chl_a	mg m ^{−3}	Chlorophyll <i>a</i> calibrated against bottle observations
b_{bp} at 470 nm b_{bp} at 650 nm b_{bp} at 660 nm b_{bp} at 700 nm	bbp470_raw bbp650_raw bbp660_raw bbp700_raw	m ^{−1}	Sea-Bird ECO Puck particulate backscattering coefficient at $\lambda = 470$ nm, 700 nm, and either 650 nm or 660 nm
b_{bp} at 470 nm corrected b_{bp} at 650 nm corrected b_{bp} at 660 nm corrected b_{bp} at 700 nm corrected	bbp470 bbp650 bbp660 bbp700	m ^{−1}	b_{bp} with additional dark subtraction of 1 st percentile of b_{bp} from 190–200 m
b_{bp} at 470 nm spike flag b_{bp} at 650 nm spike flag b_{bp} at 660 nm spike flag b_{bp} at 700 nm spike flag Chl <i>a</i> spike flag	bbp470_spikeflag bbp650_spikeflag bbp660_spikeflag bbp700_spikeflag chl_a_spikeflag	1 = spike 0 = no spike	Flag indicating b_{bp} or Chl <i>a</i> spike according to Briggs <i>et al.</i> ¹⁰
Variable QC Flag	(var)_qcflag	1 = pass 2 = input var flagged 3 = questionable 4 = bad data	Maximum qc flag (1–4) for each variable (<i>var</i>) e.g. bbp470_qcflag, temp_qcflag
Range QC Flag	qcflag_range	1, 3, or 4	Range test: qc = 3 is out of regional range qc = 4 is out of global range
Density Inversion QC Flag	qcflag_densinv	1, 3, or 4	Density inversion test: qc = 4 for salin, sigma qc = 3 for temp, cond, b_{bp} , chl_a, oxygen
Stuck QC Flag	qcflag_stuck_(var)	1, 3, or 4	Stuck value test: qc = 4 for variable dive profile
Biofoul QC Flag	qcflag_biofoul	1, 3, or 4	Biofoul test: qc = 4 for oxygen
Biofoul Bio-optics QC Flag	qcflag_biofoulOptics	1, 3, or 4	Biofoul test: qc = 4 for chl_a, b_{bp} if bad data qc = 3 chl_a, b_{bp} if questionable spikes qc = 1 if chl_a, b_{bp} unaffected
Visual QC Flag	qcflag_visual_(var)	1, 3, or 4	Visual test: qc = 3 or 4; visually bad data noted in Table 5 that is not flagged by other tests

Table 2. Seaglider variable names and descriptions.

All analyses were done using MATLAB v2021b. Sensor information (manufacturer, model number, and serial number) are provided in Table 3 for each mission.

Raw data processing. *Conductivity, temperature, and pressure.* Pressure was measured using either a Paine or Kistler sensor (Table 3). Temperature and conductivity raw signals were converted according to sensor calibration coefficients, with values outside the valid sensor range removed. Minimum and maximum sensor signal frequency ranges were taken from the calibration constants file (Conductivity Min/Max = 2.8/8.5 kHz; Temperature Min/Max = 2.8/7.0 kHz). Initial processing was done to adjust both temperature and conductivity where the data were corrected for 1st order lags¹⁵. Calculations for salinity and potential density anomaly were based on lag-corrected temperature and conductivity. Conductivity was first used to calculate practical salinity from Gibbs Seawater Toolbox (gsw_SP_from_C.m), and then converted to absolute salinity (gsw_SA_from_SP.m). Quality-controlled data were re-processed, beginning with the lag correction, in order to minimize the effects of outliers. Potential density anomaly was calculated with respect to a reference water pressure of 0 db using the Gibbs Seawater Toolbox (gsw_sigma0.m).

Seaglider, Mission #	Pressure	Conductivity, Temperature	Oxygen Optode	Chlorophyll a, bbp470, bbp700	Chlorophyll a, bbp650 or bbp660
sg146-4	Paine, 211-75-710-05, s/n 214718	Sea-Bird, s/n 0073	Aanderaa, 5013, s/n 19, Foil Batch 1707	WET Labs, BB2FL-VMG, s/n 397	WET Labs, BBFL2-VMT, s/n 400
sg146-5	Paine, 211-75-710-05, s/n 214718	Sea-Bird, s/n 0141	Aanderaa, 5013, s/n 19, Foil Batch 1707	WET Labs, BB2FL-VMT, s/n 684	WET Labs, BBFL2-VMT, s/n 400
sg146-6	Paine, 211-75-710-05, s/n 214718	Sea-Bird, s/n 0142	Aanderaa, 5013, s/n 19, Foil Batch 1707	WET Labs, BB2FL-VMT, s/n 684	WET Labs, BBFL2-VMT, s/n 400
sg146-7	Paine, 211-75-710-05, s/n 214718	Sea-Bird, s/n 0136	Aanderaa, 5013, s/n 19, Foil Batch 1023	WET Labs, BB2FL-VMT, s/n 684	WET Labs, BBFL2-VMT, s/n 400
sg146-9	Paine, 211-75-710-05, s/n 214718	Sea-Bird, s/n 0136	Aanderaa, 5013, s/n 19, Foil Batch 1023	WET Labs, BB2FL-VMG, s/n 398	WET Labs, BBFL2-VMT, s/n 400
sg147-4	Paine, 211-75-710-05, s/n 214718	Sea-Bird, s/n 0074	—	WET Labs, BB2FL-VMG, s/n 397	WET Labs, BBFL2-VMT, s/n 452
sg148-6	Paine, 211-75-710-05, s/n 241009	Sea-Bird, s/n 0075	Aanderaa, 5013, s/n 21, Foil Batch 1707	WET Labs, BB2FL-VMG, s/n 398	WET Labs, BBFL2-VMT, s/n 401
sg148-8	Paine, 211-75-710-05, s/n 241009	Sea-Bird, s/n 0075	Aanderaa, 5013, s/n 21, Foil Batch 1707	WET Labs, BB2FL-VMG, s/n 398	WET Labs, BBFL2-VMT, s/n 402
sg148-9	Paine, 211-75-710-05, s/n 241009	Sea-Bird, s/n 0075	Aanderaa, 5013, s/n 21, Foil Batch 1707	WET Labs, BB2FL-VMG, s/n 398	WET Labs, BBFL2-VMT, s/n 402
sg148-11	Paine, 211-75-710-05, s/n 241009	Sea-Bird, s/n 0075	Aanderaa, 5013, s/n 21, Foil Batch 1707	WET Labs, BB2FL-VMG, s/n 398	WET Labs, BBFL2-VMT, s/n 402
sg148-12	Paine, 211-75-710-05, s/n 241009	Sea-Bird, s/n 0154	Aanderaa, 5013, s/n 21, Foil Batch 1023	WET Labs, BB2FL-VMG, s/n 1016	WET Labs, BBFL2-VMT, s/n 402
sg148-16	Kistler, 4260M070, s/n 4939959	Sea-Bird, s/n 0141	Aanderaa, 5013, s/n 21, Foil Batch 1023	WET Labs, BB2FL-VMT, s/n 1916	WET Labs, BBFL2-VMT, s/n 402
sg511-21	Kistler, 4260M091, s/n 5292218	Sea-Bird, s/n 0131	Aanderaa, 4831, s/n 888, Foil Batch 1824M	WET Labs, BB2FL-IRB, s/n 7655	WET Labs, BBFL2-IRB, s/n 6510
sg512-1	Paine, 211-75-710-05, s/n 253669	Sea-Bird, s/n 0136	Aanderaa, 4330IE, s/n 199, Foil Batch 2808F	WET Labs, BB2FL-VMT, s/n 590	WET Labs, BBFL2-VMT, s/n 673
sg512-3	Paine, 211-75-710-05, s/n 253669	Sea-Bird, s/n 0134	Aanderaa, 4330I, s/n 199, Foil Batch 1023E	WET Labs, BB2FL-VMT, s/n 590	WET Labs, BBFL2-VMT, s/n 740
sg512-4	Paine, 211-75-710-05, s/n 253669	Sea-Bird, s/n 0066	Aanderaa, 4330I, s/n 199, Foil Batch 1023E	WET Labs, BB2FL-VMT, s/n 590	WET Labs, BBFL2-VMT, s/n 740
sg626-1	Kistler, 4260M070, s/n 4813657	Sea-Bird, s/n 0273	Aanderaa, 4331F, s/n 596, Foil Batch 1207F	WET Labs, BB2FL-VMT, s/n 1404	WET Labs, BBFL2-VMT, s/n 1405
sg626-4	Kistler, 4260M070, s/n 4813657	Sea-Bird, s/n 0273	Aanderaa, 4733, s/n 596, Foil Batch 1824E	WET Labs, BB2FL-IRB, s/n 5372	WET Labs, BBFL2-IRB, s/n 1405

Table 3. Sensor Information (Manufacturer, *Model #*, Serial #).

Oxygen optodes. Several different oxygen optodes (Aanderaa 4330, 4331, & 5013) were used to measure dissolved oxygen concentrations. The optode lumiphore is excited by a pulse of blue light, with the emitted light of the lumiphore quenched by increasing oxygen concentrations. However, the calculated oxygen concentrations are influenced by effects of temperature, salinity, pressure, and time response in addition to sensor drift¹⁶. A series of corrections was applied to the raw data to provide a quality corrected oxygen output. Processing steps detailed below align with those detailed in the Argo data processing protocol¹⁷. First, a phase pressure adjustment was applied to account for an O₂-independent effect on the lumiphore¹⁸. Next, a correction for the instrument time-response lag was applied to each dive profile of optode phase using the inverse filtering algorithm proposed by Bittig *et al.*¹⁹. We observed that the inverse filtering approach amplifies noise not present in uncorrected O₂ profiles (Fig. 3a,b). Artificially increasing the resolution of the data by interpolating onto a 1 second grid and smoothing over 60 points resolve the noise amplification (Fig. 3c). The time-response, τ , was assigned a value of 30 s for slow-response sensing foils and 20 s for fast-response sensing foils. These time delays are based on optimizations which minimize deviations between ascending and descending profiles⁸.

O₂ was then calculated as a function of optode phase and CT Sail temperature (instead of optode temperature as per recommendations). The equations used were optode model-dependent¹⁷, with an output of either O₂ concentration or partial pressure. Outputs of partial pressure were converted to O₂ concentration using temperature and salinity. Next, corrections for salinity and pressure were applied²⁰. Updated coefficients from the Benson & Krause refit²¹, as recommended by SCOR WG142²², were used for the corrections. Quality-controlled data was re-processed, beginning with the inverse filtering correction, to minimize the effects of outliers in creating artificial O₂ spikes.

Chlorophyll a and particulate backscattering coefficient. ECO Puck sensors (Sea-Bird, previously WET Labs) were used to measure Chl *a* fluorescence and the volume scattering function (VSF) at 124° (i.e. β (124°)). A factory-calibrated dark count was subtracted from the corresponding signal counts, and the difference then converted using a scale factor. The VSF was measured at three wavelengths ($\lambda = 470$ nm, 700 nm, and either 650 or 660 nm) and converted to b_{bp} by subtracting the scattering component due to seawater²³ and multiplying by $2\pi\chi$, where $\chi = 1.076$ (for scattering at an angle of 124°)²⁴. To intercompare missions, we converted the b_{bp} (660 nm) to b_{bp} (650 nm) using a spectral slope of -0.41 ²⁵. As the new values were less than 1% different, and the change an order of magnitude lower than detectable signal counts, we simply refer to b_{bp} (660 nm) as b_{bp} (650 nm) in the technical validation section.

We note some problems encountered with one of the ECO Puck sensors, and assumptions made based on our expertise. While two ECO Puck sensors (BB2FL and BBFL2) were deployed on every mission, the signals counts were often reported incorrectly for the BB2FL sensor (Chl *a*, b_{bp} 470, and b_{bp} 700). On four missions (sg512_1, sg512_3, sg512_4, and sg148_12), Chl *a* was assigned to the BB2FL temperature column.

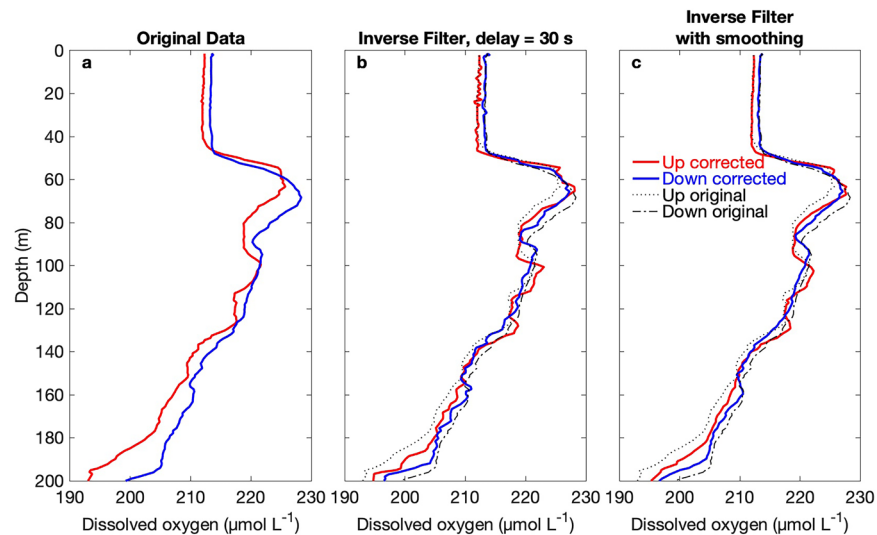


Fig. 3 Example of dissolved oxygen profiles after the inverse filtering correction. (a) Original O₂ profiles for ascending ('up' red lines) and descending ('down' blue lines) dives. (b) An inverse filtering correction (see Bittig *et al.*¹⁶) is applied to the same dives, but noise is amplified. (c) A modified inverse filtering method is applied to reduce noise amplification. Original profiles are down for reference ('up' black dotted, 'down' black dashed).

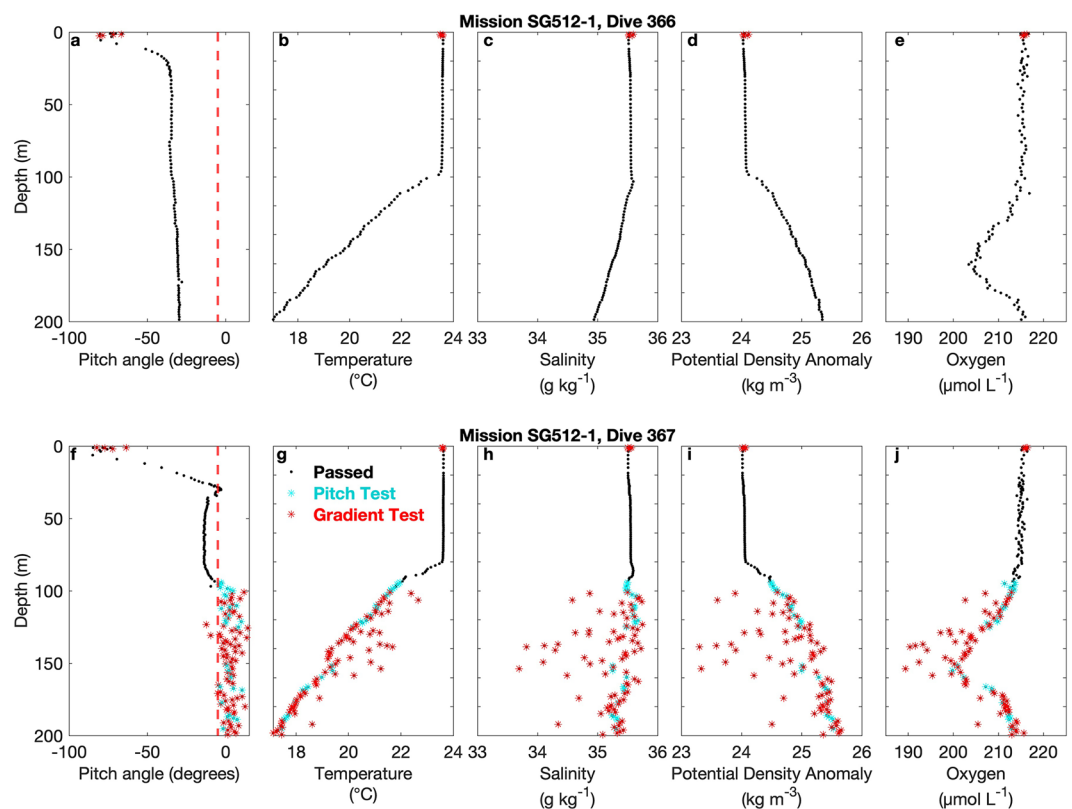


Fig. 4 Pitch density inversion test results for two profiles from Seaglider 512 mission 1 during descent. Dive profiles are shown for (a,f) pitch angle, (b,g) temperature, (c,h) salinity, (d,i) potential density anomaly, and (e,j) oxygen. Dive 366 (top row) only has flagged observations in the surface. Dive 367 (bottom row) has observations flagged below 100 m) where the pitch angle is greater than -5 degrees (vertical red line). Pitch angles flagged (cyan symbols) above 75 m are only flagged if gradient/density inversion test also flagged (red symbols).

Variable	Quality Control Flags							
	Range Test	Pitch Angle Test	Density Inversion Test	Biofoul test	Stuck Value Test	Input Variable Flagged*	Visual general	Visual sensor [†]
Temperature	0.05	1.51	2.32				0.30	0.47
Conductivity	0.31	1.51	2.32				0.30	0.47
Salinity	0.36	1.46	2.33			4.28	0.30	0.37
Potential Density Anomaly	0.18	1.46	2.33			4.30	0.30	0.37
Oxygen	0.38			12.69		4.45	0.37	11.08
Chlorophyll <i>a</i>	0.22			5.91	0.07		0.42	0.16
b_{bp} 470	1.09			6.81	1.30	4.66	0.44	1.62
b_{bp} 700	1.13			6.9	4.08	4.69	0.45	3.37
b_{bp} 650	0.53			5.95	0.33	4.96	0.42	0.04

Table 4. Percent of data flagged using each quality control step. There is some overlap as data can be flagged multiple times. Numbers reflect percent of total observations flagged across all missions. *Certain variables have inputs (e.g. salinity and temperature are required for oxygen processing), and have an additional ‘input variable flag’ if any input is flagged as questionable or bad data. [†]The percent of oxygen data flagged on the ‘visual sensor’ test primarily composes of the mission sg511-21. That mission is the second longest in this dataset, with oxygen values collected down to ~800 m, and thus a large portion of the flagged dataset.

After visually confirming profiles typical of Chl *a*, and not temperature, we corrected the column assignment on those missions. On three missions (sg146_5, sg146_5, and sg146_7) no Chl *a* signal was reported to any BB2FL data column and deemed lost. Lastly, on mission sg146_7, we found that b_{bp} 470 signal counts rolled over into b_{bp} 700 signal count column for several profiles. All b_{bp} 700 on this mission is missing or corrupted (rolled over signal counts or constant value), and removed altogether.

Quality control steps. All quality control flags were preserved in each mission file (Table 2). If a test passed the data were assigned a QC value of 1 (‘good data’). If a test failed (e.g. out of range or density inversion tests), the data were flagged, either as ‘questionable data’ (QC = 3) or as ‘bad data’ (QC = 4), and not included in data analysis. In certain cases, variables depend on an input variable during data processing. If an input variable is flagged as bad or questionable, a QC = 2 is applied for ‘input flag’. Cases are 1) salinity calculations use temperature and conductivity; 2) Potential density anomaly calculations depend on temperature, conductivity, and salinity; 3) O₂ adjustments dependent on temperature and salinity; and 4) b_{bp} dependent on temperature and salinity for the beta seawater subtraction. Analyses that are highly sensitive to minor errors (e.g. spike analysis, diel anomalies, isopycnal differences) should be wary of using data with a QC = 2 without first checking those points (see Fig. 4f–j for example). For each variable, the maximum QC value of the different tests was used to decide whether to include the data point for technical validation. No data with a QC flag > 1 were used for technical validation or calibrations. A summary of the percent data flagged with each quality control flag is provided in Table 4.

Pitch angle test (Density Inversions). Decreases in the Seaglider pitch angle can indicate a reduced ascent/descent speed and can potentially lead to detection of density inversions that are an artifact caused by the decreased flow rate. The CT Sail sensor measuring temperature and conductivity on the Seaglider is free-flushed (i.e. unpumped) and a speed reduction can lead to bias in the measurements. As a result, large spikes in salinity, and potential density anomaly can occur if temperature and/or conductivity are affected. These spikes normally occur at the bottom of the dive profile, when the glider is briefly more horizontal and moving slowly, but we also occasionally observed them in long profile sections. While a gradient or density inversion test is often employed to identify sharp spikes in CTD variables^{26,27}, we found that monitoring changes in pitch angle is the simplest method to identify sections of questionable data (Fig. 4). Density inversions (defined as potential density anomaly gradients > 0.03 kg m⁻³) failed to flag all points in sections where the density inversions were extensive. To address this problem, we flagged positive pitch angles (> 5°) for descending and negative pitch angles (< 5°) for ascending profiles (Fig. 4f–j, red symbols). Corresponding observations of temperature, conductivity, salinity, and potential density anomaly were flagged. A pitch angle flag was assigned a QC = 3, and downgraded to QC = 4 if the density inversion gradient was > 0.03 kg m⁻³. The density inversion check was repeated (without flagged points) until the total number of flagged points did not change. On descending profiles where the Seaglider slowed down, data where the pitch angle was flagged were often not associated with density inversions (Fig. 4f, 30–40 m). As such, the pitch angle flag was not used for descending profiles above 75 m. Note that salinity spikes may carry over into O₂, and create artificial spikes (Fig. 4j).

Global and regional range tests. Values outside a set global range were considered incorrect due to sensor malfunctioning and were flagged (QC = 4). The recommended minimum and maximum were based on the Argo DAC Protocol ‘Global Range Test’ (Table 5)^{26,28}. Because the Seaglider observations presented here were taken at Station ALOHA where the HOT program has collected nearly-monthly physical and biogeochemical observations since 1988, an additional ‘Regional Range Test’ was used for temperature, salinity, potential density anomaly, and O₂ (Table 5). Data outside the regional ranges were flagged (QC = 3) as questionable.

Variable	Global Range	Regional Range
Temperature (°C)	-2.5 to 40	2 to 30
Salinity (PSU)	2 to 41	33 to 35.8
Conductivity (mS/cm)	0 to 85	30 to 60*
Potential Density Anomaly (kg m^{-3})	0 to 60	21 to 28
Oxygen ($\mu\text{mol L}^{-1}$)	0 to 600	0 to 240
Optode Phase (counts)	none	10 to 70
Chlorophyll- <i>a</i> (mg m^{-3})	-0.5 to 50	none
b_{bp} 470 (m^{-1})	-0.1 to 0.1	none
b_{bp} 650 (m^{-1})	-4e-2 to 4e-2	none
b_{bp} 700 (m^{-1})	-4e-2 to 4e-2	none

Table 5. Range limits applied during quality control processing. Global range values are taken from the Argo global range test. Regional range values are specific to Station ALOHA. *Conductivity regional limits are based on salinity and temperature values.

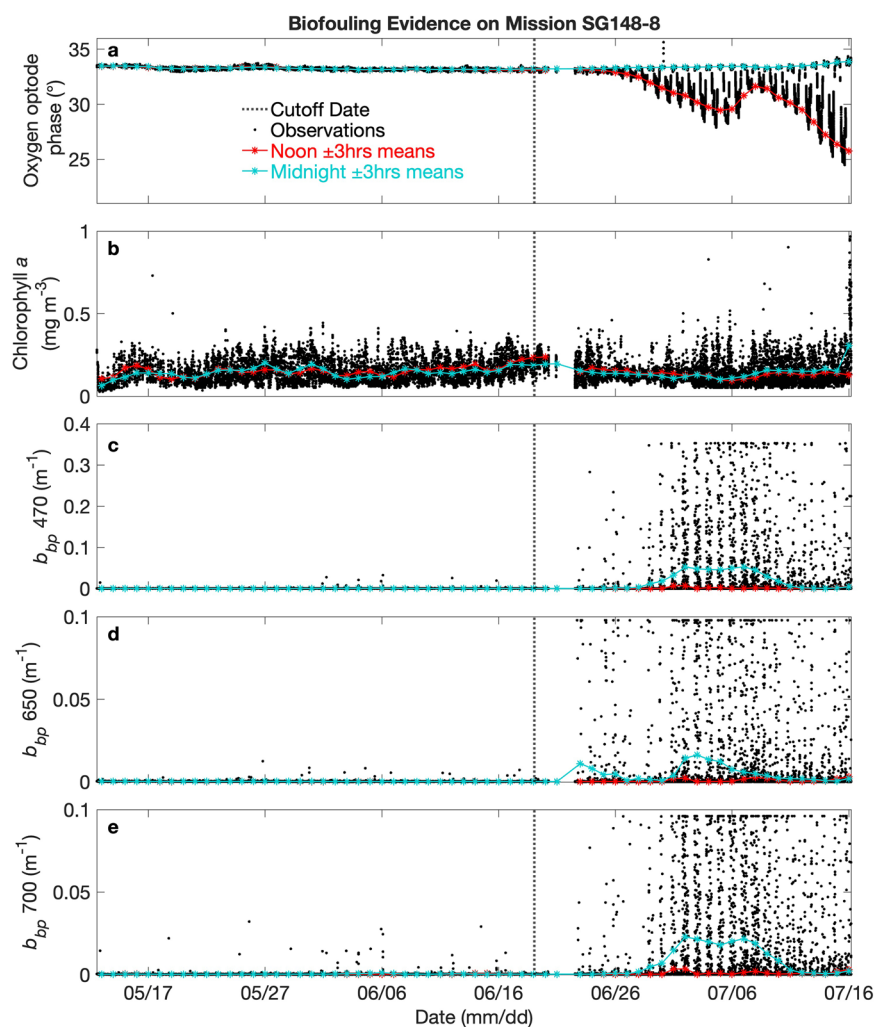


Fig. 5 Evidence of biofouling during mission 8 of Seaglider 148. (a) Midday (red) and midnight (cyan) O_2 optode phase means in the upper 40 m diverge after the cutoff date (06/18). Deep, 190–200 m, observations of (b) Chl *a*, (c) b_{bp} (470 nm), (d) b_{bp} (650 nm), and (e) b_{bp} (700 nm) plotted as well. Values after the cutoff date are clearly elevated during nighttime (Chl *a* and b_{bp} at all wavelengths).

Stuck value test. In some instances, a sensor has a repeating value throughout the dive profile with no natural variability. We identified these profiles using a “Stuck Value Test”^{26,28}. If more than 40% of a profile contains an

Seaglider, Mission #	Date Cutoff	Bio-optics flagged
sg146-5	19-Oct-2010	No indication of chl <i>a</i> or b_{bp} sensor fouling
sg146-6	05-Jul-2011	Yes, noticeable spike increase QC = 3
sg148-8	24-Jun-2009	Yes, all bio-optics data is classified as QC = 4
sg148-9	04-Jan-2011	Yes, noticeable spike increase QC = 3
sg512-3	05-Oct-2012	No indication of chl <i>a</i> or b_{bp} sensor fouling

Table 6. Biofouling date cutoffs. On indicated missions, all oxygen optode data is flagged after the cutoff date. Bio-optics (Chlorophyll *a* and b_{bp} channels) are visually checked for an increase in spikes to indicate sensor fouling, and flagged depending on severity. Chlorophyll *a* and b_{bp} observations that show no change after the cutoff dates are not flagged.

Sensor	Visual mission-by-mission flag notes
General/All sensors	sg146-4: dives 194:359 glider sensor failure, noted evidence of shark bite damage on glider recovery
	sg148-11: dives 1:120 glider had pitch issue and appeared off course prior to 6/27/12
CT Sail	Outlier dives flagged: sg146-5 (dives 595, 268), sg146-6 (dive 187), sg146-7 (dive 66), sg146-9 (dive 12), sg148-6 (dive 411), sg148-9 (367), sg148-16 (dive 165), sg511-21 (dives 90, 894)
	Outlier points flagged: sg146-4, sg146-7, sg148-6, sg148-11, sg148-12, sg148-16, sg512-3
Aanderaa Optode	sg147-4: sensor failed in first few days, all O ₂ flagged
	sg511-21: noticeable O ₂ drift after 17 May 2023
	sg626-4: outlier dive flagged (dive 1)
BB2FL	bbp470 outliers flagged: sg148-11 (dives 100-186), sg512-3 drift (dives 475+)
	bbp700 outlier flagged: sg148-11 (dives 100-186), sg512-4 outlier points
BBFL2	Chl <i>a</i> outliers flagged: sg146-9 (dives 177-195), sg511-21 (dive 351), sg512-3 (dives 643-646)
	bbp650 outliers flagged: sg511-21 outlier points

Table 7. List of visual flags for all missions. The following datasets are flagged after initial quality control checks are run, and dives are visually checked for suspicious outliers.

identical value, the entire profile was flagged as bad data (QC = 4). Raw signal counts were used for bio-optical data, as variability can be introduced in data processing steps (e.g., seawater scattering subtraction for b_{bp}).

Biofouling evidence test. Biofilms on the sensors may result in large signals in O₂ and bio-optical measurements (Chl *a*, b_{bp}) over a prolonged time-period, as observed during several missions. Fouling occurred more often on missions which spent more time in shallower water (<200 m). Identifying the shifts early avoids bad measurements feeding into calibrations steps. We developed a simple test to automate identification of measurements affected by biofouling (Fig. 5). When fouling affected the oxygen optode measurements, O₂ (optode phase) was significantly higher (lower) at midday than at midnight in the mixed layer. Differences in O₂ decreased below the mixed layer and disappeared below the DCM. We believe that this was caused by the production of oxygen in proportion to ambient light near the sensing membrane by the biofouling phytoplankton attached to the foil. As a test, the daily difference in the mean optode phase measured by the Aanderaa optode around midday (± 3 hours) and midnight (± 3 hours) in the top 40 m was calculated. If the daily difference in phase is greater than 0.1 °, the first instance is flagged as the biofouling date. If midday and midnight means past the biofouling date are significantly different (ANOVA, p -value < 0.05), the O₂ data are flagged as bad (QC = 4). Bio-optical sensors were not always affected by biofouling, and thus a visual check was performed on the bio-optical data from 190–200 m (Fig. 5b–e). We did not develop a reliable bio-optical test, and therefore relied on visual inspection of data before and after the biofouling cut-off date. Bio-optical values with exceptionally high spikes (e.g. b_{bp} 470 > 0.1 m⁻¹, and b_{bp} 700 > 0.04 m⁻¹) were flagged as bad data (QC = 4), a moderate increase in spikes as questionable (QC = 3), and no apparent change as QC = 1. A full summary of the missions in which biofouling was observed, biofouling cut off dates, and the bio-optical flags is summarized in Table 6.

Visual QC Flag. Lastly, all datasets were visually inspected for remaining outliers. These data were flagged as questionable (QC = 3) or bad (QC = 4) depending on the severity (Table 7) and not included in further analysis, which is described below.

Additional processing (Calibrations, Corrections). *Oxygen Winkler calibration.* Nearby profiles of shipboard Winkler bottle oxygen observations were matched to a Seaglider optode dissolved O₂ concentration profile (Fig. 6). Calibration points used were collected within two days of the Seaglider observation, within 10 km where possible, and no deeper than 100 m. This depth range (0–100 m) was chosen to prioritize the upper euphotic zone. If no calibration match-ups were found the distance criterion was expanded outward in 10 km intervals with a maximum of 30 km. Dissolved oxygen concentrations were corrected by multiplying by a gain correction factor²⁹ calculated as the mean ratio of Winkler O₂ to Seaglider O₂ (Table 8). We did not attempt a sensor drift correction as the gliders used for the missions reported here did not have a method to conduct in-air

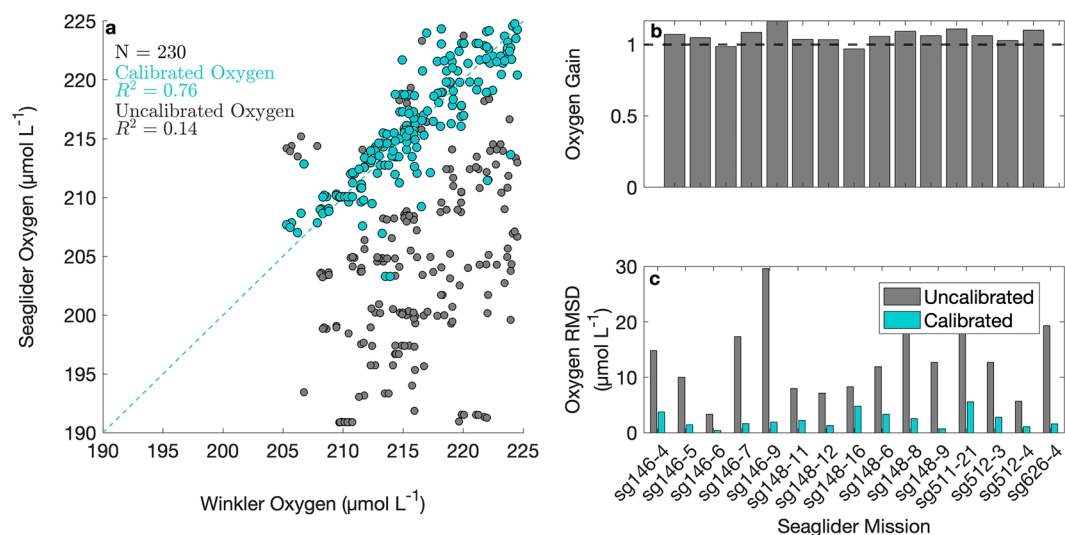


Fig. 6 Winkler calibration for oxygen optodes. (a) Calibrated Seaglider oxygen observations (cyan symbols) fall on the 1:1 dashed line, while uncalibrated Seaglider observations (grey symbols) generally underestimate O_2 . (b) Gain factors (Winkler O_2 : optode O_2) are above 1 for all but two Seaglider missions. (c) Root mean square deviations (RMSD) between Winkler and Seaglider observations are calculated for uncalibrated (grey bars) and calibrated (cyan bars) values. Discrete Winkler observations are from cruises in the vicinity of Station ALOHA, bounded by the red box in Fig. 2.

Seaglider, Mission ^a	Oxygen Gain	Chlorophyll HPLC Calibration			Backscattering Deep Dark Count (m^{-1})			
		Chl <i>a</i> slope (mg m^{-3})	Chl <i>a</i> intercept (mg m^{-3})	Chl <i>a</i> slope factor	$b_{bp, 470 \text{ nm}}$	$b_{bp, 650 \text{ nm}}$	$b_{bp, 660 \text{ nm}}$	$b_{bp, 700 \text{ nm}}$
sg146-4	1.07	0.53 [§]	5.85E-02	1.27	2.12E-04		1.28E-04	1.25E-05
sg146-5	1.05	0.89 [§]	2.63E-03	1.01	5.63E-05		6.03E-05	1.22E-04
sg146-6	0.98	0.37 [§]	5.72E-02	1.68	5.49E-05		7.12E-05	1.44E-04
sg146-7	1.09	0.67 [§]	-1.26E-02	1.57	-2.07E-05		4.21E-06	
sg146-9	1.16	1.14 [†]	5.57E-02	0.62	2.79E-04		4.86E-05	1.10E-04
sg147-4		0.76 [†]	-1.58E-03	1.29	5.27E-04	1.99E-04		3.26E-04
sg148-6	1.06	0.97 [†]	-3.31E-02	1.15	2.06E-04		2.93E-04	1.69E-04
sg148-8	1.09	0.76 [§]	-5.72E-03	1.27	4.43E-04	3.22E-04		9.78E-04
sg148-9	1.06	0.81 [§]	2.90E-02	1.04	1.49E-04	1.98E-05		2.49E-04
sg148-11	1.03	0.79 [†]	5.45E-02	0.82	-2.42E-04	9.68E-05		5.43E-06
sg148-12	1.03	0.67 [§]	4.09E-02	1.04	3.78E-04	6.34E-05		1.44E-04
sg148-16	0.97	0.78 [§]	2.58E-02	1.03	3.03E-04	-1.44E-04		1.86E-04
sg511-21	1.11	0.76 ^{*,§}	2.20E-02	1.22	3.03E-04	4.11E-04		2.65E-04
sg512-1	1.18	0.50 [§]	8.76E-02	0.94	3.34E-04	-5.49E-04		1.40E-04
sg512-3	1.06	0.56 [§]	5.59E-02	1.24	-1.13E-04	-7.12E-05		3.73E-05
sg512-4	1.03	0.78 [§]	4.54E-02	0.91	-2.91E-04	-1.54E-04		5.68E-05
sg626-1	1.22	0.60 [§]	4.31E-02	1.26	3.01E-04	1.92E-04		1.79E-04
sg626-4	1.08	0.85 ^{*,†}	3.04E-02	1.04	2.74E-04	1.72E-04		1.65E-04
mean	1.08	0.73	3.09E-02	1.13	1.75E-04	4.66E-05	1.01E-04	1.93E-04

Table 8. Summary of corrections applied to oxygen optodes, Chl *a* fluorescence, and particulate backscattering coefficients. Dissolved O_2 concentrations are multiplied by gain values based on Winkler bottle observations. Chl *a* fluorescence is corrected against a linear regression to HPLC Chl *a* pigment concentrations. The dimensionless slope factors (Seaglider Chl *a*: HPLC Chl *a*) are shown for reference to Roesler *et al.*³⁰ and not used for calibrations. Particulate backscattering coefficients (b_{bp}) have a seawater dark count subtraction taken as the 2nd percentile of signal counts near 200 m. Empty cells indicate no data were collected from the sensor for that variable. *HPLC Chl *a* observations unavailable, Fluorometric Chl *a* used instead. [†]FLBB2 fluorometer Chl *a* reported. [§]FL2BB fluorometer Chl *a* reported.

oxygen observations. We observed that two winter missions equipped with a fast-response foil (sg512-1 and sg626-1) showed high variability, and had mixed layer values above and below the Winkler observations during the entire 30+ year HOT program. The O_2 measurements collected during these missions were subsequently flagged (QC = 3) and not included in the technical validation analyses presented below.

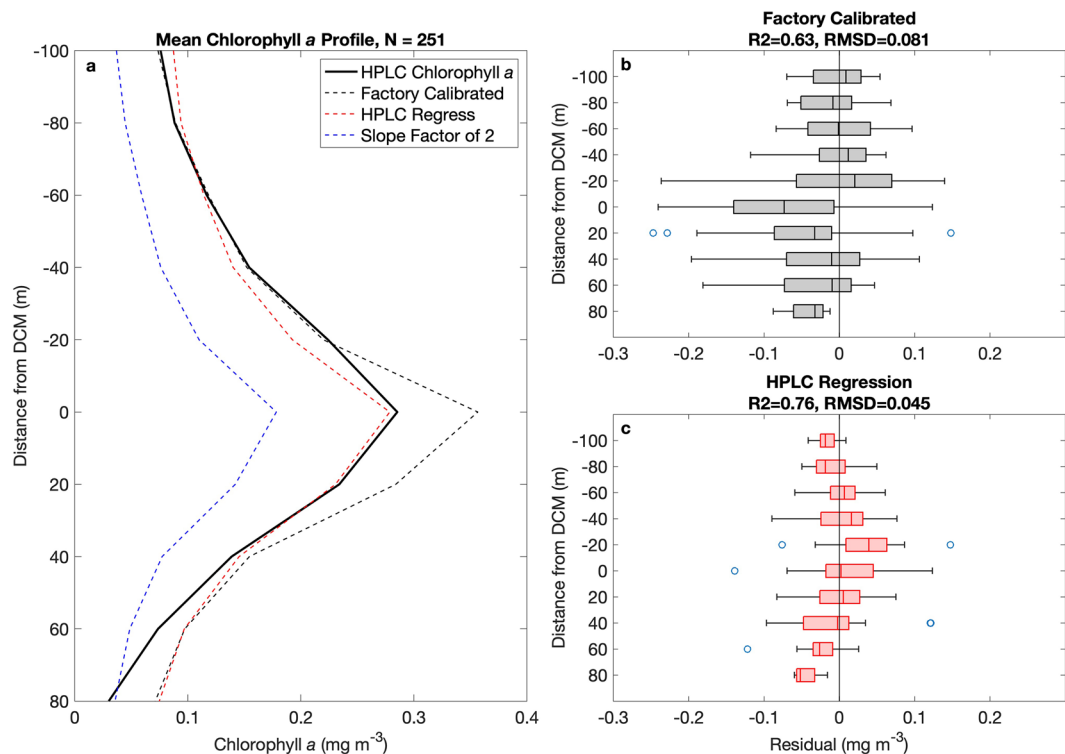


Fig. 7 Chl *a* HPLC calibration. Mean Chl *a* profiles shown in (a) for HPLC Chl *a* observation (solid black line), Seaglider Chl *a* using factory calibration coefficients (black dashed line), Seaglider Chl *a* corrected with slope factor of 2 (blue dashed line), and Seaglider Chl *a* corrected with HPLC linear regression (red dashed line). Residuals (HPLC Chl *a* – Seaglider Chl *a*) from the (b) Factory calibrated $F_{chl a}$ (grey boxplots) are minimized using (c) HPLC regression coefficients (red boxplots). On each boxplot, the central mark indicates the median, and the left and right edges of the box indicate the 25th and 75th percentiles, respectively. The whiskers extend to the most extreme data points not considering outliers, and the outliers (i.e. values more than 1.5 the interquartile range away from the top or bottom of the box) are plotted individually as open blue circles.

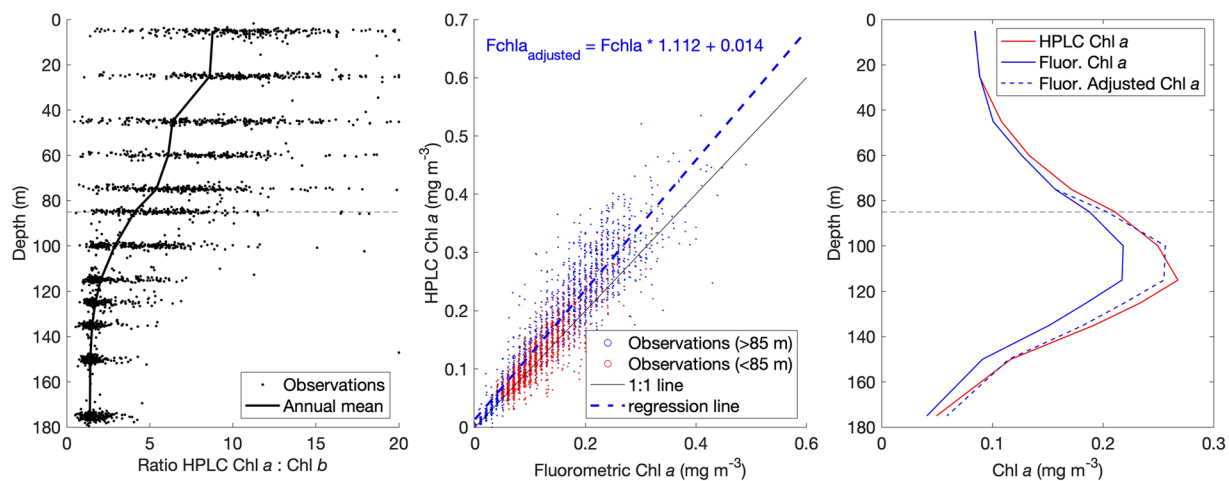


Fig. 8 Fluorometric Chl *a* correction for calibrations. Standard methods of determining Fluorometric Chl *a* at Station ALOHA do not account for the contribution of Chl *b* and may therefore underestimate Chl *a* concentrations. The ratio of Chl *a* to Chl *b* decreases with depth (left). Chl *a* concentrations derived from HPLC measurements significantly correlate with fluorometrically determined Chl *a* (p -value < 0.0001), but are typically higher (center), especially at increasing depths where the relative contribution of Chl *b* to total Chl is higher. To account for this disagreement, we adjusted all Fluorometric Chl *a* concentrations using the linear regression between HPLC and Fluorometric Chl *a* concentrations derived from HOT observations. Only measurements deeper than 85 m (black dashed reference line in left, right panels) were used for the regression and adjusted. The adjusted Fluorometric Chl *a* concentrations are in good agreement with HPLC Chl *a* measurements (right). For the 2023 Seaglider missions, the adjusted Fluorometric Chl *a* observations were used for calibration.

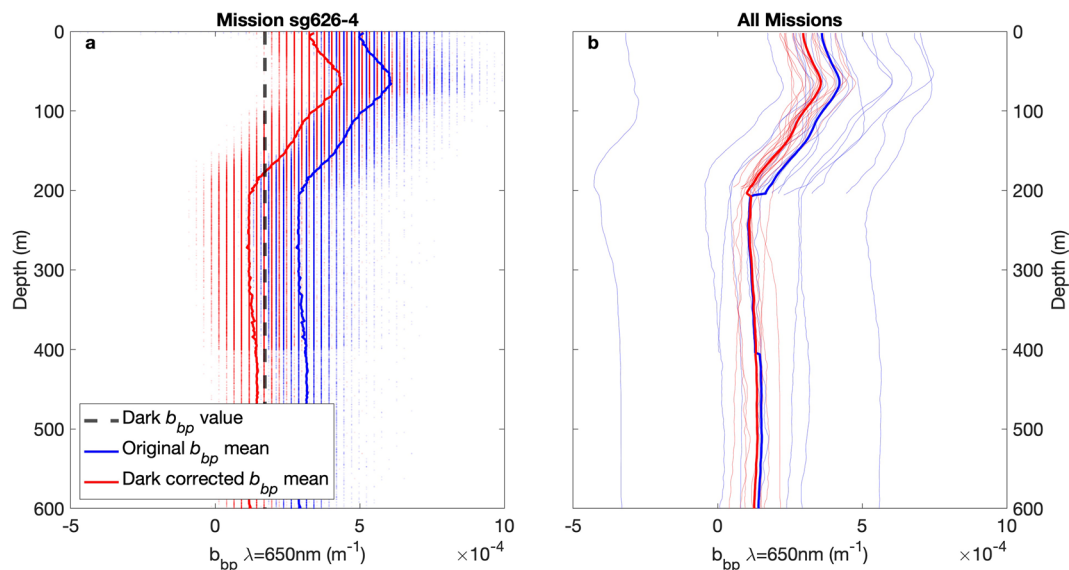


Fig. 9 Dark corrected particulate backscattering coefficient, b_{bp} (650 nm), profiles. **(a)** An example correction is shown for sg626-4, where the original data after factory calibration (blue points) are corrected (red points) using a deep dark count (black dashed vertical line). **(b)** All mission mean b_{bp} profiles are shown for original data (light blue lines) and dark corrected data (light red lines). The mean of all missions is shown in bold of the same respective color.

Chlorophyll *a* calibration. Seaglider Fluorescence ($F_{chl a}$) was converted to Chl *a* using the coefficients provided by the manufacturer. However, the values often diverged from *in situ* Chl *a* concentrations measured in the laboratory on seawater collected from a ship near the gliders, particularly close to the depth of the deep chlorophyll maximum (DCM) (Fig. 7). The factory calibrated scale factor of $F_{chl a}$: Chl *a* is based on a uniform phytoplankton culture, and the conversion could under- or over-estimate the $F_{chl a}$: Chl *a* of diverse, regional phytoplankton communities³⁰. While it is common practice to use a global bias correction of dividing Chl *a* from *in situ* fluorometers by 2^{30,31}, this global correction consistently underestimated Chl *a* at Station ALOHA (Fig. 7a, blue dashed profile), and overall performed worse than the factory calibration. Instead, we found the Sea-Bird ECO Puck (previously WET Labs) only slightly overestimated Chl *a* (Table 8: mean slope factor = 1.13 ± 0.26 , $N = 18$). Our regional estimate for Station ALOHA is consistent with Roesler *et al.* (see their Fig. 5)³⁰, where the authors observed slope factors nearer to 1 in the North Pacific Subtropical Gyre. However, no single slope factor was consistently good for all Seaglider missions (Table 8: range 0.62–1.68), and the positive bias in glider Chl *a* near and below the DCM remains. For this reason, we used available shipboard measurements of Chl *a* collected near the Seagliders to accurately calibrate the Seaglider $F_{chl a}$ on a mission-by-mission basis.

We used only nighttime $F_{chl a}$ values for sensor calibration because daytime fluorescence underestimates Chl *a* values due to non-photochemical quenching³². The HOT program measures Chl *a* concentration, after filtration and extraction of pigments in acetone, using two complementary methods: high-performance liquid chromatography (HPLC) and fluorometric pigment analysis (<https://hahana.soest.hawaii.edu/hot/protocols/protocols>). HPLC Chl *a* observations were chosen over fluorometric determinations of Chl *a*, as fluorometric analysis can underestimate Chl *a* in the presence of Chl *b*^{33,34}, which is particularly concentrated near the depth of the DCM at Station ALOHA³⁵. Seaglider Chl *a* was corrected using a linear regression to HPLC Chl *a* (MATLAB ‘robustfit.m’ function with Huber loss function to minimize influence of outliers). Because the linear regression was sensitive to the displacement of the DCM, which can oscillate tens of meters in a few hours due to internal waves³⁶, we used distance from DCM instead of depth to match up observations. For the HPLC Chl *a*, we identified the DCM using an *in situ* fluorometer on CTD upcasts when the sample was collected. Residuals were minimized for the HPLC regressed Chl *a* ($R^2 = 0.76$, RMSD = 0.045) compared to the factory calibrated Chl *a* ($R^2 = 0.63$, RMSD = 0.081) (Fig. 7b,c). For recent missions with no HPLC observations yet available (2023 missions), we used the Fluorometric Chl *a* measurements instead of HPLC Chl *a* for calibration. When using Fluorometric Chl *a*, we employed a linear correction for the contribution of chlorophyll *b* to absorption for all measurements below 85 m (Fig. 8; slope = 1.112, offset = 0.014 mg m^{-3}). While the Seagliders were equipped with two fluorometers, we only report the sensor with highest coverage of unflagged data, or else with the lowest RMSD. We did not correct for non-photochemical quenching in the dataset presented, and thus only used nighttime profiles for technical validation.

Particulate backscattering coefficient. *In Situ* dark count subtraction. Dark counts depict the signal measured by the sensor in the absence of scattering and they are known to differ from the values provided by the manufacturer. A common solution is to additionally subtract a glider-specific dark count from all measurements, which is assumed to be close to the lowest signal measured below the euphotic layer (e.g. 5th percentile from 200–400 m³⁷; 0.05th percentile from >400 m¹²). Less than half of the Seaglider missions presented here had b_{bp}

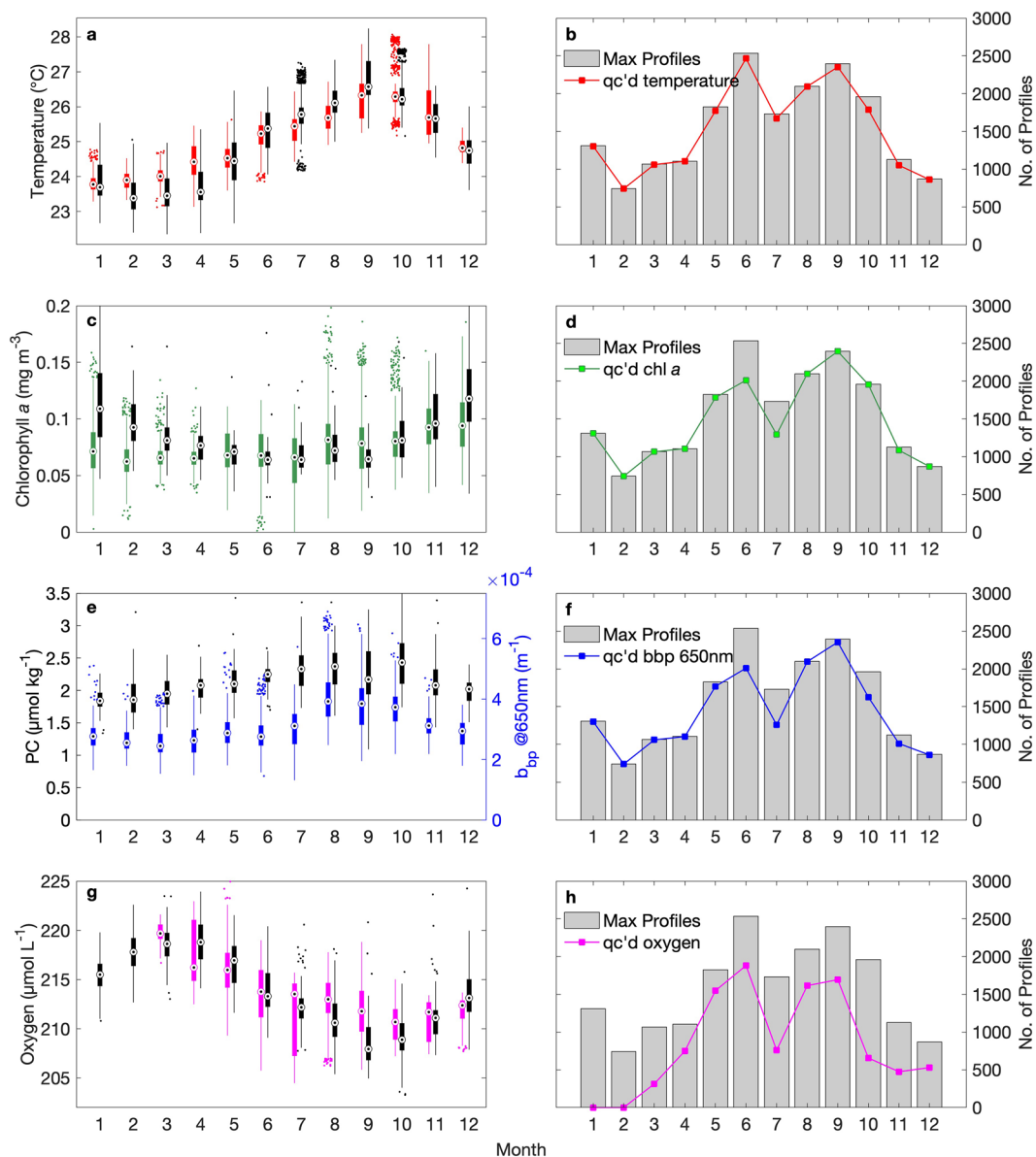


Fig. 10 Upper ocean (25 m) monthly climatology for key variables. Monthly observations and number of quality controlled (qc'd) profiles are plotted for **(a,b)** temperature (red), **(c,d)** Chl *a* (green), **(e,f)** b_{bp} (650 nm) (blue), and **(g,h)** oxygen (magenta). Hawaii Ocean Time-series monthly climatology (1988–2021; black boxplots) include 5 m and 25 m bottle collections for HPLC Chl *a*, particulate carbon (PC) and Winkler oxygen, and upper 5–25 m for CTD temperature data. On each boxplot, the central mark indicates the median, and the bottom and top edges of the box indicate the 25th and 75th percentiles, respectively. The whiskers extend to the most extreme data points not considering outliers (marker points above and below center line position). Values more than 1.5 the interquartile range away from the top or bottom of the box are considered outliers. Number of max profiles is including datasets with observations in the upper 25 m only and may be lower than totals in Table 1.

observations below 200 m (Table 2). To use a consistent approach across missions, we used the 1st percentile of b_{bp} from 190–200 m as a secondary dark count, which was subtracted from all b_{bp} measurements during each mission. Post correction, the b_{bp} profiles clustered together, but were lower than the uncorrected profile (Fig. 9). A justification for this correction is that b_{bp} data on a similar AUV platform (Wirewalkers) collected in the vicinity of Station ALOHA (<https://doi.org/10.5281/zenodo.3750468>), also using a Sea-Bird ECO Puck, does not vary substantially between missions³⁸.

Spike identification. Large spikes in b_{bp} were flagged as described in Briggs *et al.*¹⁰ A baseline b_{bp} was found by applying a 7-point moving minimum filter followed by a 7-point moving maximum filter. Spikes were identified by subtracting this baseline, and flagged if the spike was 2x larger than the 90th percentile of deep spikes (190–200 m). This depth range is modified from Briggs *et al.*¹⁰ and chosen for consistency among Seaglider missions.

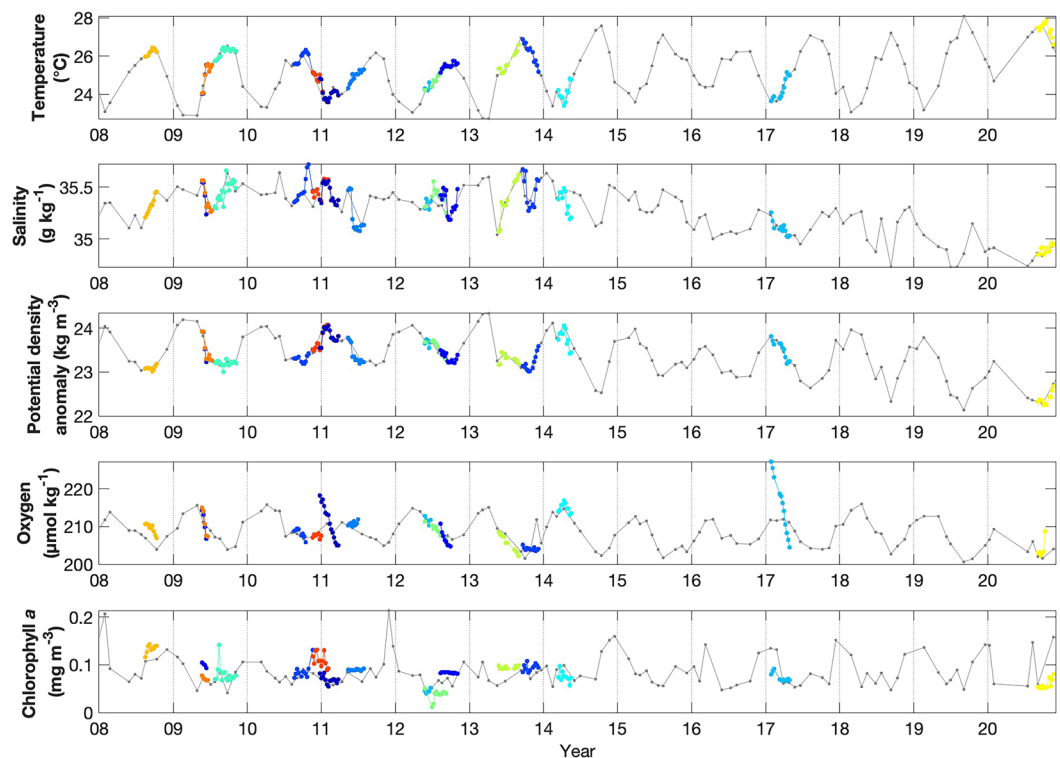


Fig. 11 Interannual upper 25 m HOT and Seaglider time-series. HOT observations are in grey and Seaglider observations (binned monthly) are shown as colored dots, with the color indicating different missions. HOT observations for 2023 are preliminary and not included in this figure.

The b_{bp} presented below is de-spiked, where flagged b_{bp} spikes are not included in data analysis in the Technical Validation section. A similar analysis was performed on Chl a , but spikes were more infrequent and not removed from the Chl a profiles. All spike flags are retained as a separate data variable (Table 2).

Data Records

The processed data described here are publicly available at Zenodo (<https://doi.org/10.5281/zenodo.14680626>)¹⁴. Dataset v1.2 has been peer reviewed. For each mission there is a xlsx file containing only quality controlled data, as well as two netCDF files, one with all data and the other one with all quality control flags. Raw data files for all Seaglider missions are publicly available at the time of collection: <https://hahana.soest.hawaii.edu/seagliders/>. The raw data files were subsequently processed as described in the methods section and quality controlled. Quality-controlled data (QC = 1) are also available on the Simons Collaborative Marine Atlas (CMAP) website (<https://simonscmap.com/>) as separate xlsx files. Information about the different missions is provided in Table 1. A complete list of variables associated with each file is given in Table 2. MATLAB Code used for data processing is available at GitHub (<https://github.com/cathygarcia/SeagliderDataprocessing>).

Technical Validation at Station ALOHA

Quality-controlled Seaglider observations (QC flag = 1) are validated against observations from the HOT program at Station ALOHA. Within the NPSG, Station ALOHA is characterized by warm and nutrient-depleted surface waters year-round, but does experience seasonality³⁹. Seasons are defined accordingly; winter (December–February), spring (March–May), summer (June–August), and fall (September–November)¹. Winter conditions are characterized by a deeper mixed layer depth (MLD), more uniform seawater properties vertically, and relatively elevated MLD Chl a linked to photoacclimation. In the late spring and summer, the interaction of seasonal light, nutrients, and phytoplankton leads to a decrease in MLD Chl a in non-bloom conditions, but a deepening and enhancement of the DCM⁴⁰. During this same period, O_2 decreases near the surface because of the reduced solubility combined with the exchange of gas with the atmosphere while it increases below the mixed layer, where the lack of air-sea exchanges allows the accumulation of the O_2 produced from the positive net community production⁴¹. Particulate carbon accumulation in the euphotic zone and enhanced carbon export occurs during late summer months, especially, and into the fall¹. While the 30+ years Station ALOHA climatology (1988–2021) is based on near monthly sampling frequency, the Seagliders aperiodically sampled Station ALOHA over a 15-year period (2008–2023). Differences between the climatologies may represent stochastic events sampled at high-resolution by the Seagliders, or differences attributed to sampling periods.

Independent estimates of temperature, salinity, and potential density anomaly were obtained using HOT CTD observations matched to Seaglider observations ($n = 2,454$). The nearest Seaglider profile within a 2-day window was selected for each HOT CTD profile, and observations were matched to the nearest depth

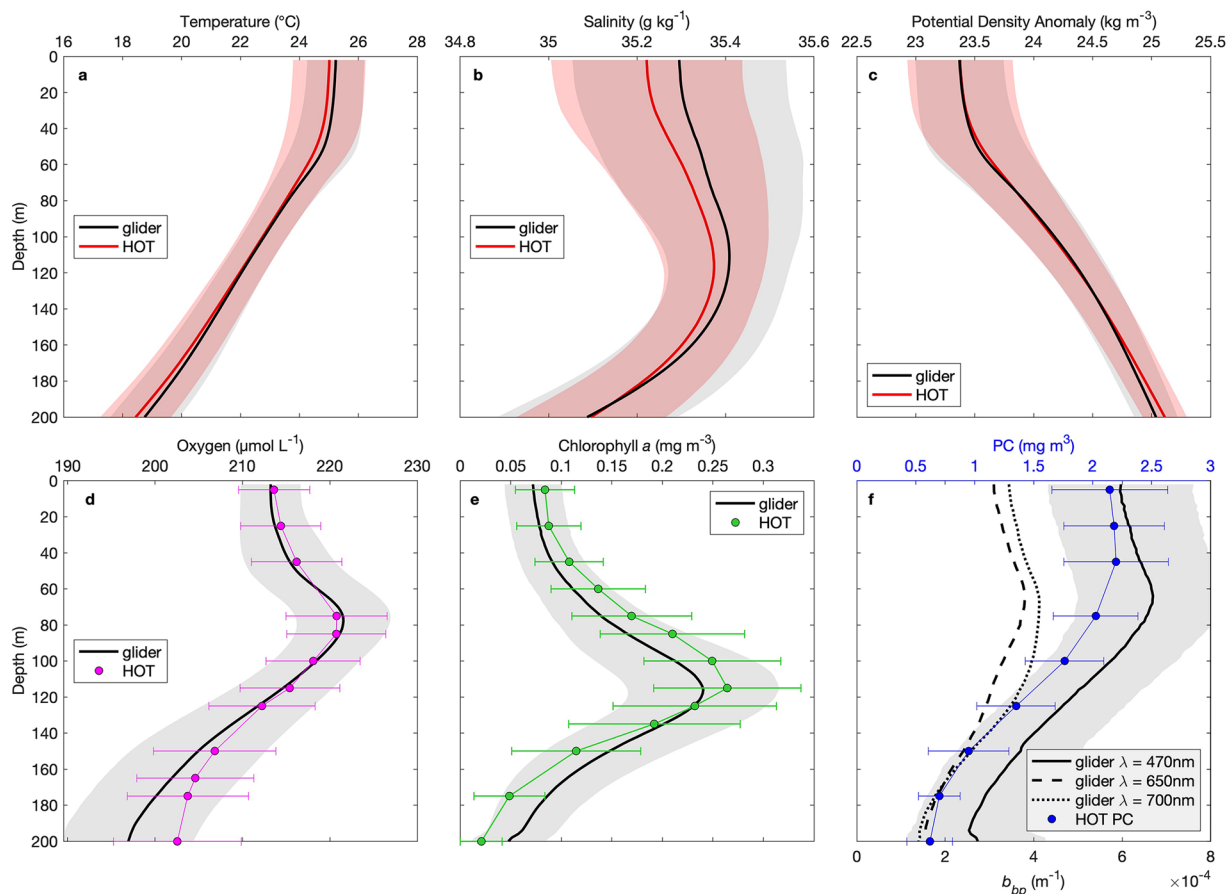


Fig. 12 Annual mean depth profiles. HOT (1988–2021) annual mean \pm std (red lines and shading) profiles are shown for CTD (a) temperature, (b) salinity, and (c) potential density anomaly and HOT bottle data for (d) Winkler oxygen (magenta points), (e) HPLC Chl *a* (green points), and (f) particulate carbon, PC (blue points). Bottle data mean \pm std are calculated at standard cruise sampling depths. Corresponding glider mean \pm std profiles (black line and shading) are also shown, with particulate backscatter coefficient (b_{bp}) data in (f) at three wavelengths. Only mean profiles (and not \pm std) are shown for b_{bp} at 650 nm (black dashed line) and 700 nm (black dotted line).

(maximum 2 m difference). Quality controlled Seaglider data are significantly correlated for temperature ($R^2 = 0.97$, $p < 0.0001$), salinity ($R^2 = 0.92$, $p < 0.0001$), and potential density anomaly ($R^2 = 0.98$, $p < 0.0001$). Calibrated optode oxygen concentrations are significantly correlated to HOT Winkler oxygen observations (Fig. 6, $R^2 = 0.76$, $p < 0.0001$, $n = 230$). The weaker correlation may partly be explained by time and space lags between bottle observations and Seaglider profiles. Restricting matches (time lag < 1 day, distance within 5 km) results in an improved fit ($R^2 = 0.92$, $p < 0.0001$, $n = 38$). Lastly, calibrated Chl *a* concentrations are significantly correlated to HPLC Chl *a* (Fig. 7, $R^2 = 0.76$, $p < 0.0001$, $n = 251$). Particulate backscatter coefficient has no equivalent in the HOT dataset but is compared in the following section to particulate carbon concentrations (PC) instead. We next combine Seaglider data from all 18 missions, and place the data onto a 2 m grid at annual, monthly, and bi-weekly scales to obtain a ‘Seaglider climatology.’

Monthly mixed layer climatology. The monthly seasonality of Seaglider observations in the MLD have similar ranges and seasonal patterns to those derived from HOT observations (Fig. 10). It should be noted that the HOT climatology expands the coverage of the Seaglider dataset, with measurements going back to 1988 (Fig. 11). MLDs at Station ALOHA are deeper in winter (HOT = 42 m, Glider = 39 m), and shallower in the summer months (HOT = 32 m, Glider = 30 m). Colder, oxygenated waters in the winter and early spring have higher Chl *a* (due to photoacclimation), and lower particulate matter, as suggested by b_{bp} . Warmer water and lower O_2 concentration correspond to lower Chl *a* and a build-up of particulate matter in late summer and early fall. Lower Chl *a* measured in January by the Seagliders compared to the HOT record, can partly be explained by inter-annual variation during winter 2010/11, when upper ocean Chl *a* peaked a month earlier in December (Fig. 11). The coverage of the quality controlled Seaglider dataset presented here includes more than 1000 profiles each month for all variables except for dissolved oxygen. The latter is due to the removal of O_2 data from Seaglider missions 626-1 and 512-1 which results in the lack of observations available for the months of January and February. Dissolved O_2 observations using the Aanderaa optode sensor are correlated to Winkler bottle concentrations in all but the

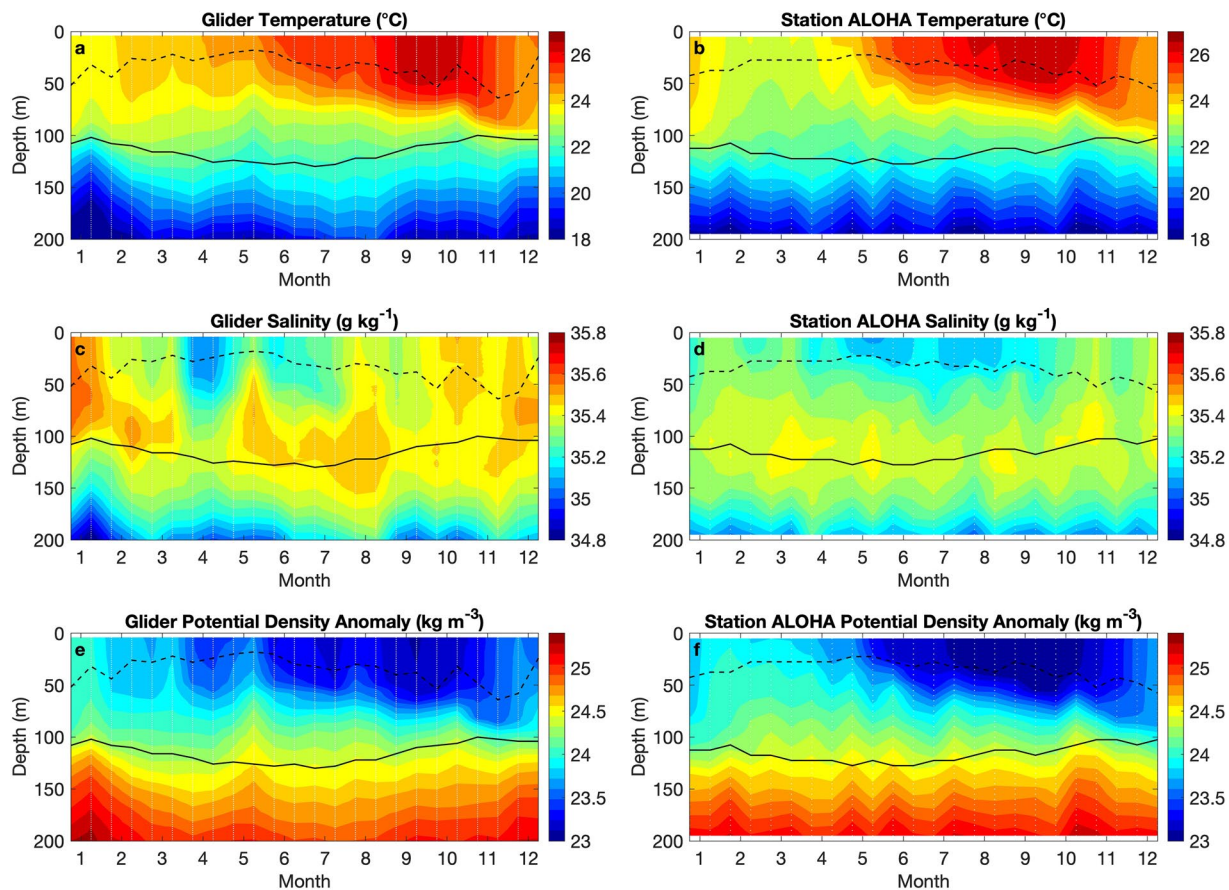


Fig. 13 Biweekly hydrography climatology in the upper 200 m. Seaglider (2008–2023) and Station ALOHA (1988–2021) profiles are averaged biweekly for (a,b) temperature, (c,d) absolute salinity, and (e,f) potential density anomaly. HOT observations are from CTD profiles at Station ALOHA. The solid black lines in (a–f) are the depths of the deep chlorophyll maximum; and dashed black lines are the mixed layer depths based on density criterion of de Boyer Montégut *et al.*⁴⁸. Figures were made using *contourf.m* on gridded profiles (white dots) in MATLAB.

two winter months, when the optodes mounted fast-response foils, and which exhibit increased sensor noise and significant variability outside the 30+ time-series observed at Station ALOHA (Fig. 11, years 2011 and 2017). At present, we cannot account for the source of the discrepancies between the fast-response foils and the HOT record, but the issue is likely related to a drift in sensor performance causing anomalous O_2 decline during the two glider missions. The drift is evident from the time-series of O_2 near the sea surface, where gliders measured a much larger variability than repeated shipboard observations at Station ALOHA (Fig. 11).

Annual and climatological depth profiles. *Hydrography (temperature, salinity, and potential density anomaly).* Seaglider parameters for hydrographical (temperature, salinity, and potential density anomaly) recreate both the mean annual (Fig. 12) and climatological seasonal variations (Fig. 13) at Station ALOHA. While the Seaglider hydrographical values are highly correlated to HOT observations, we note the annual and inter-seasonal profiles for salinity are relatively elevated. Most of the Seaglider observations presented here were collected during 2008–2014, a period of higher salinity for Station ALOHA relative to the entirety of the time-series (Fig. 11). Excluding HOT observations outside this time-period (2008–2014) reduces the variability between HOT and Seaglider climatology for both salinity and potential density anomaly (data not shown).

Oxygen & Bio-optics (Chl a and b_{pp}). Seagliders measure the same patterns and magnitudes of O_2 accumulation and loss as shipboard-based bottle values (Figs. 10, 14). Dissolved O_2 concentrations are well mixed down to 100 m through early spring. This period is followed by the formation of a subsurface O_2 peak above the DCM and below the mixed layer in the summer, and by the accumulation of particulate matter in the upper 100 m. In the fall, as the mixed layer deepens, the O_2 subsurface maximum erodes gradually and gets ventilated. The mean profile of dissolved O_2 diverges from HOT observations by an average of $3.1 \mu\text{mol L}^{-1}$ between 125–200 m (Fig. 12d) and this bias is unlikely to be due to the missing winter months. As mentioned above, both the lag and calibration steps are optimized for the upper euphotic zone and may lead to mismatches for deeper values.

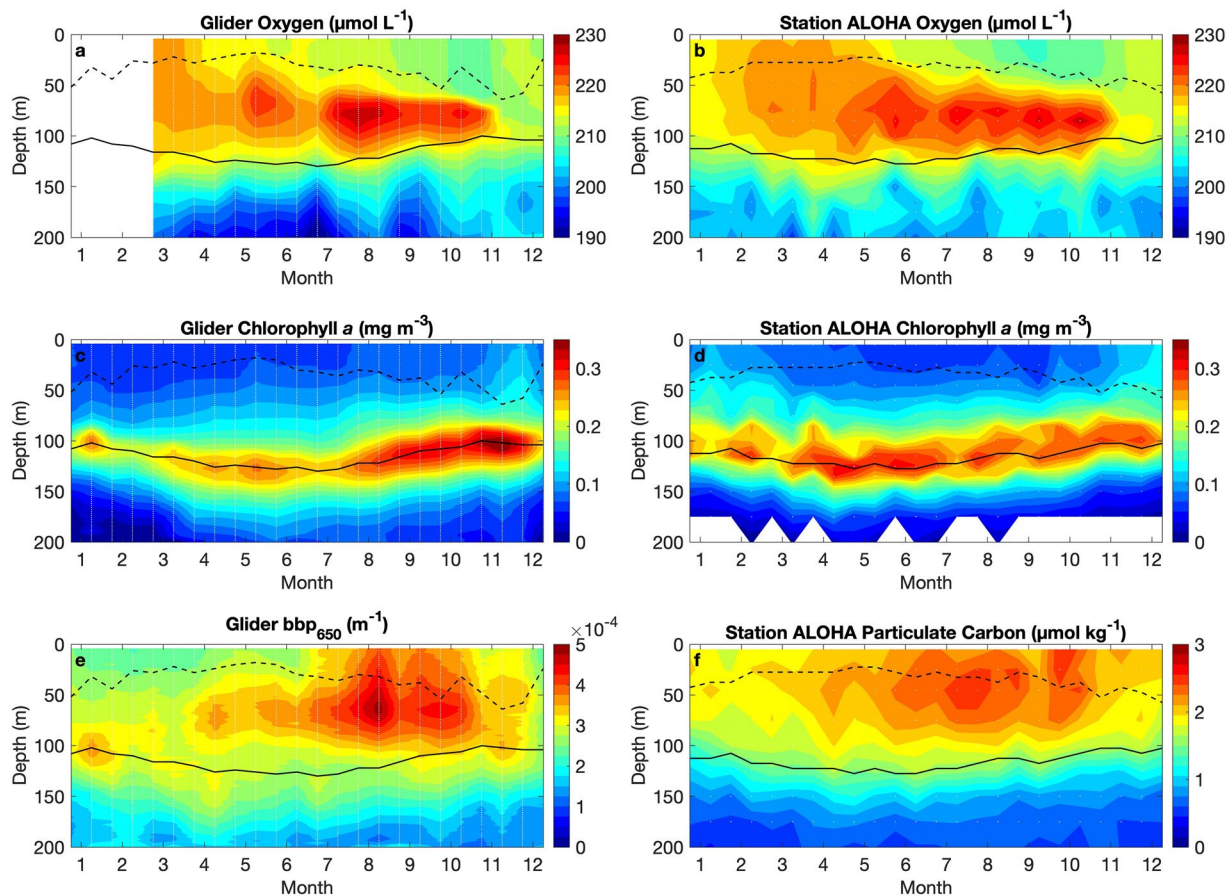


Fig. 14 Biweekly oxygen, chlorophyll *a*, particulate backscattering and particulate carbon climatology in the upper 200 m. Seaglider (2008–2023) and Station ALOHA (1988–2021) profiles are averaged bi-weekly for (a,b) oxygen, (c,d) chlorophyll *a*, (e) b_{bp} at 650 nm (Seaglider only), and (f) particulate carbon (Station ALOHA only). HOT observations are from discrete Winkler oxygen, HPLC chlorophyll *a*, and particulate carbon bottle collections at Station ALOHA. The solid black lines in (a–f) are the depths of the deep chlorophyll maximum; and dashed black lines are the mixed layer depths based on density criterion of de Boyer Montégut *et al.*⁴⁸. Figures were made using *contourf.m* on gridded profiles (white dots) in MATLAB.

Variable	Sensor Reported Precision	Sensor Reported Accuracy	Reported Argo Uncertainties	10–20 m Nighttime SD Estimated Precision	RMSD Estimated Accuracy
Temperature (°C)	0.001	0.002	0.002, Wong <i>et al.</i> ⁴²	0.008 ± 0.003	0.16 ± 0.15
Conductivity (mS cm ⁻¹)	1.00E-04	0.003	—	0.008 ± 0.003	0.13 ± 0.17
Salinity (g kg ⁻¹)	0.001	0.004	0.01 psu, Wong <i>et al.</i> ⁴²	0.003 ± 0.001	0.043 ± 0.044
Oxygen (μmol L ⁻¹)	<1	<8	1.0–1.5 μmol kg ⁻¹ , 0.5% O ₂ sat., Bittig <i>et al.</i> ¹⁶	0.093 ± 0.042	2.34 ± 1.49
Chlorophyll <i>a</i> (mg m ⁻³)	0.023 ± 0.014	0.025	0.12 ± 40% Johnson <i>et al.</i> ⁴³	0.012 ± 0.01	0.042 ± 0.01
b_{bp} 470 (m ⁻¹)	1.86E-5 ± 1.09E-5	—	2E-4, ±20% Poteau <i>et al.</i> ⁴⁴	9.45E-05 ± 2.38E-05	—
b_{bp} 650 (m ⁻¹) b_{bp} 660 (m ⁻¹)	2.96E-5 ± 7.19E-6	—	2E-4, ±20% Poteau <i>et al.</i> ⁴⁴	4.75E-05 ± 7.54E-06	—
b_{bp} 700 (m ⁻¹)	3.32E-5 ± 8.51E-6	—	2E-4, ±20% Poteau <i>et al.</i> ⁴⁴	4.83E-05 ± 1.07E-05	—

Table 9. Sensor uncertainty estimates. Reported values for sensor precision and accuracy are presented as a single value if constant across all calibration sheets, or as a mean ± standard deviation if not. Argo uncertainties are summarized in Bittig *et al.*⁴⁵, but individual sources are listed in the table. As a comparison with sensor precision values, 10–20 m nighttime mean standard deviation (SD). Root mean standard deviation (RMSD) values for hydrography (temperature, conductivity, and salinity), oxygen and Chl *a* are compared to nearby shipboard CTD, Winkler, and HPLC measurements, respectively. Here, SD and RMSD are presented as averages ± SD for all missions, but mean values for each mission are included in the dataset.

Measurements of Chl *a* closely match observed trends at Station ALOHA. Seaglider Chl *a* data reflects the decrease of shallow Chl *a* during warmer more stratified, and higher sunlight months, as well as an enhancement and deepening of the DCM in summer (Fig. 14). The mean annual profile of HOT Chl *a* is within the range observed by the Seagliders (Fig. 12e). At and above the DCM, HOT Chl *a* is greater than the Seaglider annual

mean by $\sim 0.03 \text{ mg m}^{-3}$, and HOT Chl *a* is on average lower than Seaglider Chl *a* below 140 m by $\sim 0.015 \text{ mg m}^{-3}$. Our calibrated Seaglider observations show a seasonal underestimation of Chl *a* at the DCM in spring, and overestimation in the fall. Further work is needed to improve the accuracy of Chl *a* calibrations, especially in low chlorophyll regions such as subtropical gyres.

Comparison of particulate backscattering coefficients to particulate carbon (PC) show the net accumulation of particulate material during the late summer. We do not attempt to convert b_{bp} to PC in this presentation, but note similarities in their seasonality and depth distribution. All three annual profiles of b_{bp} are high in the mixed layer with a maximum below 60 m, and gradually decrease to 200 m (Fig. 12f). Mean profiles of b_{bp} remain low below the euphotic zone, though the depth of minimum b_{bp} differs among missions and wavelengths. PC has an annual maximum in the upper 40 m (Fig. 12f), but exhibits a seasonal subsurface maximum in the spring and summer (Fig. 14). While b_{bp} is correlated to PC among annual means (b_{bp} at 470 nm $R^2 = 0.96$, 650 nm $R^2 = 0.88$, and 700 nm $R^2 = 0.83$), and biweekly means (b_{bp} at 470 nm $R^2 = 0.79$, 650 nm $R^2 = 0.78$, 700 nm $R^2 = 0.69$), direct matchups have weaker positive correlations (i.e. lower R^2).

Uncertainty estimates. We provide a range of sensor error estimates as reported in the factory calibration sheets, in previously published reports, and calculated based on sensor stability throughout missions and comparison with nearby shipboard observations (Table 9). Sensor precisions and accuracies for each mission are taken from the factory calibration sheets reported on the HOT Program website (<https://hahana.soest.hawaii.edu/seagliders/sensors/calibration.php>). Reported Argo uncertainties are listed for comparison for temperature and salinity⁴², O₂¹⁶, Chl *a*⁴³, and particulate backscattering^{44,45}. We attempt to approximate sensor precision by calculating a standard deviation of sensor values in a depth layer (10–20 m) across nighttime profiles. We chose this layer as representative of the mixed layer, but excluded the top 10 m layer due to increase noise introduced by the penetration of bubbles. In addition, we excluded daytime profiles to avoid any noise introduced by any potential interference with sunlight. The resulting precisions should be considered upper bound estimates as they include natural variability. Lastly, we estimate accuracy by comparing against nearby shipboard observations and calculating the RMSD. Hydrography values (temperature, conductivity, absolute salinity) are compared against CTD profiles, while O₂ and Chl *a* are compared against discrete Winkler and HPLC measurements, respectively, as described above. Note that side-by-side validation profiles were rarely collected, so calculated accuracies are also upper bound estimates that include any temporal and spatial variability. Even at the scale of a few kilometers, this variability may exceed sensor accuracy.

Code availability

Code and data used to reproduce all data processing are available in the GitHub repository (<https://github.com/cathygarcia/SeagliderDataprocessing>).

Received: 5 December 2023; Accepted: 12 February 2025;

Published online: 16 April 2025

References

- Karl, D. M. *et al.* Seasonal-to-decadal scale variability in primary production and particulate matter export at Station ALOHA. *Progr. Oceanogr.* **195**, 102563 (2021).
- Karl, D. M. & Lukas, R. The Hawaii Ocean Time-series (HOT) program: Background, rationale and field implementation. *Deep-Sea Res. Part II: Top. Stud. Oceanogr.* **43**, 129–156 (1996).
- Kavanaugh, M. T. *et al.* Seascapes as a new vernacular for pelagic ocean monitoring, management and conservation. *ICES J. of Mar. Sci.* **73**, 1839–1850 (2016).
- Laws, E. A. & Maiti, K. The relationship between primary production and export production in the ocean: Effects of time lags and temporal variability. *Deep-Sea Res. Part I: Oceanogr. Res. Papers* **148**, 100–107 (2019).
- Nicholson, D. P., Wilson, S. T., Doney, S. C. & Karl, D. M. Quantifying subtropical North Pacific gyre mixed layer primary productivity from Seaglider observation of diel oxygen cycles. *Geophys. Res. Lett.* **42**, 4032–4039 (2015).
- Johnson, K. S. & Bif, M. B. Constraint on net primary productivity of the global ocean by Argo oxygen measurements. *Nat. Geosci.* **14**, 769–774 (2021).
- Stoer, A. C. & Fennel, K. Estimating ocean net primary productivity from daily cycles of carbon biomass measured by profiling floats. *Limnol. Oceanogr. Lett.* **8**, 368–375 (2023).
- Barone, B., Nicholson, D., Ferrón, S., Firing, E. & Karl, D. The estimation of gross oxygen production and community respiration from autonomous time-series measurements in the oligotrophic ocean. *Limnol. Oceanogr. Meth.* **17**, 650–664 (2019).
- Omand, M. M. *et al.* Eddy-driven subduction exports particulate carbon from the spring bloom. *Science* **348**, 222–225 (2015).
- Briggs, N. *et al.* High-resolution observations of aggregate flux during a sub-polar North Atlantic spring bloom. *Deep-Sea Res. Part I: Oceanogr. Res. Papers* **58**, 1031–1039 (2011).
- Briggs, N., Dall’Olmo, G. & Claustre, H. Major role of particle fragmentation in regulating biological sequestration of CO₂ by the oceans. *Science* **367**, 791–793 (2020).
- Bol, R., Henson, S. A., Rumyantseva, A. & Briggs, N. High-frequency variability of small-particle carbon export flux in the Northeast Atlantic. *Global Biogeochem. Cycles* **32**, 1803–1814 (2018).
- Eriksen, C. C. *et al.* Seaglider: A long-range autonomous underwater vehicle for oceanographic research. *IEEE J. Oceanic Eng.* **26**, 424–436 (2001).
- Garcia, C., Barone, B., Ferrón, S., Poulos, S. & Karl, D. Multiple years of Seaglider observations of hydrography, dissolved oxygen, chlorophyll *a*, and optical backscatter at Station ALOHA (v1.2). *Zenodo* <https://doi.org/10.5281/zenodo.14680626> (2023).
- Pelland, N. A., Eriksen, C. C. & Cronin, M. F. Seaglider surveys at Ocean Station Papa: Circulation and water mass properties in a meander of the North Pacific Current. *J. Geophys. Res. Oceans* **121**, 6816–6846 (2016).
- Bittig, H. C. *et al.* Oxygen optode sensors: principle, characterization, calibration, and application in the ocean. *Front. Mar. Sci.* **4**, 429 (2018).
- Thierry, V. *et al.* Processing Argo oxygen data at the DAC level, v2.3.3. <https://doi.org/10.13155/39795> (2021).
- Bittig, H. C., Fiedler, B., Fietzek, P. & Körtzinger, A. Pressure response of Aanderaa and Sea-Bird oxygen optodes. *J. Atm. Oceanic Tech.* **32**, 2305–2317 (2015).

19. Bittig, H. C., Fiedler, B., Schloz, R., Krahnemann, G. & Körtzinger, A. Time response of oxygen optodes on profiling platforms and its dependence on flow speed and temperature. *Limnol. Oceanogr. Meth.* **12**, 617–636 (2014).
20. Garcia, H. E. & Gordon, L. I. Oxygen solubility in seawater: better fitting equations. *Limnol. Oceanogr.* **37**, 1307–1312 (1992).
21. Benson, B. B. & Krause, D. The concentration and isotopic fractionation of oxygen dissolved in freshwater and seawater and equilibrium with the atmosphere. 1: Oxygen solubility in seawater. *Limnol. Oceanogr.* **29**, 620–632 (1984).
22. Bittig, H. C. *et al.* SCOR WG 142: Quality control procedures for oxygen and other biogeochemical sensors on floats and gliders. Recommendation on the conversion between oxygen quantities for Bio-Argo floats and other autonomous sensor platforms. <https://doi.org/10.13155/45917> (2018).
23. Zhang, X., Hu, L. & He, M.-X. Scattering by pure seawater: Effect of salinity. *Opt. Express* **17**, 5698 (2009).
24. Sullivan, J. M., Twardowski, M. S., Ronald, J., Zaneveld, V., & Moore, C. C. Light Scattering Reviews 7: Radiative Transfer and Optical Properties of 189 Atmosphere and Underlying Surface; *Ch. 6 Measuring optical backscattering in water*, p. 189–224. (Springer Berlin Heidelberg 2013).
25. Centinić, I. *et al.* Particulate organic carbon and inherent optical properties during 2008 North Atlantic Bloom Experiment. *J. Geophys. Res. Oceans* **117**, C06028 (2012).
26. Wong, A., Keeley, R., Carval, T. & Argo Data Management Team. Argo quality control manual for CTD and trajectory data. <https://doi.org/10.13155/33951> (2023).
27. Woo, L. M. & Gourcuff, C. Delayed mode QA/QC best practice manual version 3.0. Hobart, Australia, Integrated Marine Observing System. <https://doi.org/10.26198/5c997b5fdc9bd> (2021).
28. Schmechtig, C., Thierry, V. & The Bio Argo Team. Argo quality control manual for biogeochemical data. *Bio-Argo group*. <https://doi.org/10.13155/40879> (2016).
29. Nicholson, D. P. & Feen, M. L. Air calibration of an oxygen optode on an underwater glider. *Limnol. Oceanogr. Meth.* **15**, 495–502 (2017).
30. Roesler, C., Uitz, J., Claustre, H. & others. Recommendations for obtaining unbiased chlorophyll estimates from *in situ* chlorophyll fluorometers: A global analysis of WET Labs ECO sensors. *Limnol. Oceanogr. Meth.* **15**, 572–585 (2017).
31. Schmechtig, C., H. Claustre, A. Poteau, & F. D’Ortenzio. BGC-Argo quality control manual for the Chlorophyll-A concentration. <https://doi.org/10.13155/35385> (2018).
32. Cullen, J. J. The deep chlorophyll maximum: comparing vertical profiles of chlorophyll a. *Can. Journ. Fish. Aquat. Sci.* **39**, 791–803 (1982).
33. Holm-Hansen, O. & Riemann, B. Chlorophyll a determination: Improvements in methodology. *Oikos* **30**, 438 (1978).
34. Welschmeyer, N. A. Fluorometric analysis of chlorophyll a in the presence of chlorophyll b and pheopigments. *Limnol. Oceanogr.* **39**, 1985–1992 (1994).
35. Bricaud, A. Natural variability of phytoplanktonic absorption in oceanic waters: Influence of the size structure of algal populations. *J. Geophys. Res.* **109**, C11010 (2004).
36. Letelier, R. M. *et al.* Temporal variability of phytoplankton community structure based on pigment analysis. *Limnol. Oceanogr.* **38**, 1420–1437 (1993).
37. Thomalla, S. J., Moutier, W., Ryan-Keogh, T. J., Gregor, L. & Schütt, J. An optimized method for correcting fluorescence quenching using optical backscattering on autonomous platforms. *Limnol. Oceanogr.* **16**, 132–144 (2018).
38. Barone, B. & Karl, D. M. ALOHA Wirewalker dataset (1.0) [Dataset] <https://doi.org/10.5281/zenodo.3750468> (2020).
39. Karl, D. M. & Church, M. J. Ecosystem structure and dynamics in the North Pacific Subtropical Gyre: New views of an old ocean. *Ecosystems* **20**, 433–457 (2017).
40. Letelier, R. M., Karl, D. M., Abbott, M. R. & Brigare, R. R. Light driven seasonal patterns of chlorophyll and nitrate in the lower euphotic zone of the North Pacific Subtropical Gyre. *Limnol. Oceanogr.* **49**, 508–519 (2004).
41. Shulenberger, E. & Reid, J. L. The Pacific shallow oxygen maximum, deep chlorophyll maximum, and primary productivity, reconsidered. *Deep-Sea Res. Part A. Oceanogr. Res. Papers.* **28**, 901–919 (1981).
42. Wong, A. P. S. *et al.* Argo data 1999–2019: two million temperature-salinity profiles and subsurface velocity observations from a global array of profiling floats. *Front. Mar. Sci.* **7**, 700 (2020).
43. Johnson, K. S. *et al.* Biogeochemical sensor performance in the SOCCOM profiling float array. *J. Geophys. Res. Oceans.* **122**, 6416–6436 (2017).
44. Poteau, A., Boss, E. & Claustre, H. Particulate concentration and seasonal dynamics in the mesopelagic ocean based on the backscattering coefficient measured with Biogeochemical-Argo floats. *Geophys. Res. Lett.* **44**, 6933–6939 (2017).
45. Bittig, H. C. *et al.* A BGC-Argo guide: planning, deployment, data handling and usage. *Front. Mar. Sci.* **6**, 502 (2019).
46. Stommel, H. Varieties of oceanographic experience. *Science* **139**, 572–6 (1963).
47. Dickey, T. D. The emergence of concurrent high-resolution physical and bio-optical measurements in the upper ocean and their applications. *Rev. Geophys.* **29**, 383–413 (1991).
48. de Boyer Montégut, C., Madec, G., Fischer, A. S., Lazar, A. & Iudicone, D. Mixed layer depth over the global ocean: An examination of profile data and a profile-based climatology. *J. Geophys. Res. Oceans* **109**, C12003 (2004).

Acknowledgements

We extend a large thanks to the captains and crew of our primary deployment or recovery vessels, such as the R/V *Kilo Moana*, R/V *Ka’Imikai-O-Kanaloa*, *Ms. Mahi*, Chartered *Red Raven* (Parker Marine Inc), along with the chief scientists and UH Ocean Technology Group who have assisted with Seaglider missions since 2008. Successful on site deployment and recovery operations on site were completed by Blake Watkins, Tara Clemente, Tim Burrell, Ryan Tabata, Brandon Brenes, and Eric Shimabukuro. Lance Fujiaki provided invaluable support via near real-time observational plotting, and long term data storage and handling. Original data processing code was graciously provided by David ‘Ro’ Nicholson. Ancillary data for calibration and comparison were collected by many hands (scientists, technicians, students, and numerous others) as part of the HOT program since 1988, funded by multiple NSF OCE awards and PIs. Finally, we acknowledge the generous funding by the Gordon and Betty Moore Foundation (award #3794 to D.M.K.), the National Science Foundation through their support of the Daniel K. Inouye Center for Microbial Oceanography: Research and Education (EF0424599 to D.M.K.), and the Simons Collaboration on Processes and Ecology (SCOPE; awards 329108, 721252 and 721264 to D.M.K.). Reprocessing of the data, as well as B.B. and S.F., were funded by National Science Foundation (OCE-2048435).

Author contributions

The Seaglider study was originally conceived by D.M.K., while B.B. and S.F. proposed the re-analysis and intercomparison described herein. D.M.K., B.B. and S.F. supervised the investigation. S.P. orchestrated all preparation for Seaglider missions, piloting, data handling, and Seaglider maintenance between missions. C.A.G. and B.B. developed the data processing methodology. C.A.G. wrote a draft and made figures with substantial input from B.B., S.F., S.P., and D.M.K.

Competing interests

The authors declare no competing interests.

Additional information

Correspondence and requests for materials should be addressed to C.A.G.

Reprints and permissions information is available at www.nature.com/reprints.

Publisher's note Springer Nature remains neutral with regard to jurisdictional claims in published maps and institutional affiliations.



Open Access This article is licensed under a Creative Commons Attribution-NonCommercial-NoDerivatives 4.0 International License, which permits any non-commercial use, sharing, distribution and reproduction in any medium or format, as long as you give appropriate credit to the original author(s) and the source, provide a link to the Creative Commons licence, and indicate if you modified the licensed material. You do not have permission under this licence to share adapted material derived from this article or parts of it. The images or other third party material in this article are included in the article's Creative Commons licence, unless indicated otherwise in a credit line to the material. If material is not included in the article's Creative Commons licence and your intended use is not permitted by statutory regulation or exceeds the permitted use, you will need to obtain permission directly from the copyright holder. To view a copy of this licence, visit <http://creativecommons.org/licenses/by-nc-nd/4.0/>.

© The Author(s) 2025